IFT WAT

ELPROMA

Światłowodowy interferometr pętlowy jako układ czujnikowy – przegląd możliwości aplikacyjnych

Leszek R. Jaroszewicz

Instytut Fizyki Technicznej, Wojskowa Akademia Techniczna
ul. gen. Sylwestra Kaliskiego 2, 00-908 Warszawa
Elproma Elektronika Sp z o. o.
ul. Duńska 2A, 05-152 Czosnów

20th Conference on Optical Fibers and Their Applications, Lublin 11-14.09.2023

Plan wystąpienia

- Rys historyczny i nie tylko
- Żyroskop światłowodowy FOG jako „urealnienie” efektu Sagnaca
- Sejsmograf rotacyjny – nie tak znany kuzyn FOG
- System ochrony rozległych obiektów – pamięci Prof. Szustakowskiego
- W pełni światłowodowy polarymetr,
- Układ lustra (reflektora) światłowodowego - FLM:
  - określanie parametrów włókien,
  - pomiar współczynnika załamania ośrodka,
- Splatane fotony w służbie FOG.

Interferometric transfer function

Bulk optic Fiber optic

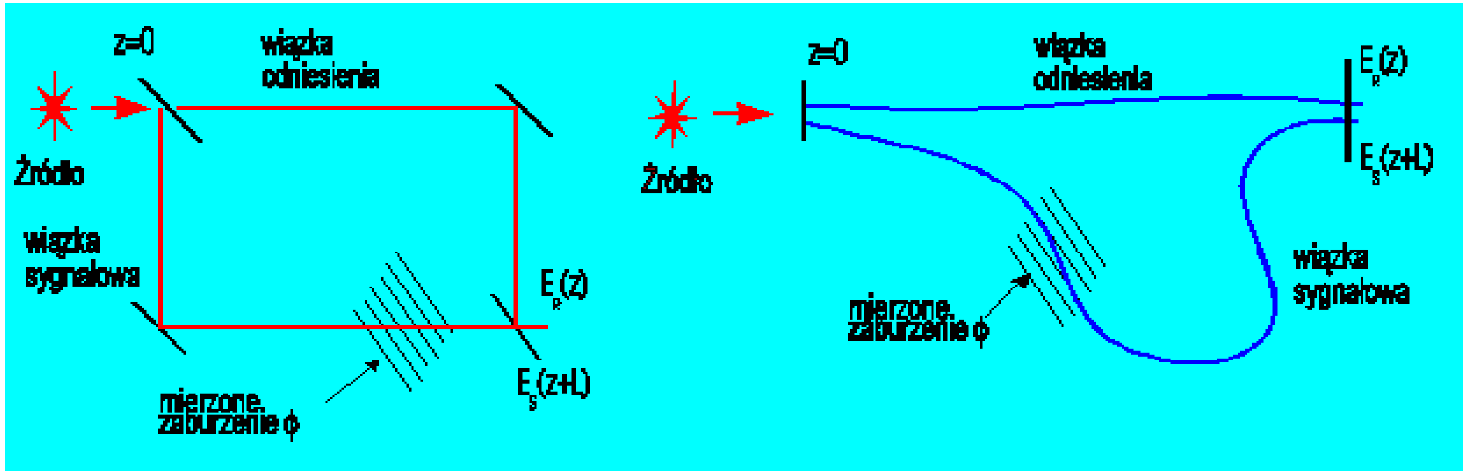

$I = I'\{1 \pm V(\gamma)cos[\phi - \phi_0(\gamma)]\}$ $I = I'\{1 \pm V(\gamma, SOP)cos[\phi - \phi_0(\gamma, SOP)]\}$

The Kapron theorem of equivalence:

$$\boldsymbol{M_s} \stackrel{\text{def}}{=} \boldsymbol{R}(\alpha)\boldsymbol{G}(\delta)\boldsymbol{R}(\xi)$$

Jones vector for source:

$$\boldsymbol{E}_{in} = \begin{bmatrix} cos\beta \\ sin\beta e^{i\Delta} \end{bmatrix}$$

System mattrix:

$$\boldsymbol{m} = \boldsymbol{E}_{in}^{+} M_R^{+} M_S \; \boldsymbol{E}_{in} \in C$$

$$I = I'\{1 \pm Abs(\boldsymbol{m})cos[f(\phi) - arg(\boldsymbol{m})]\}$$

Sensitivity Configuration Bias

Loop configuration:

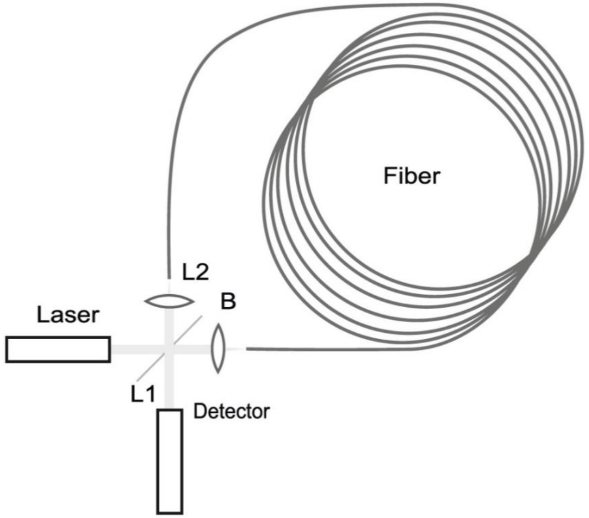

Only twist $\boldsymbol{M_s}=\boldsymbol{R}[\alpha]$:

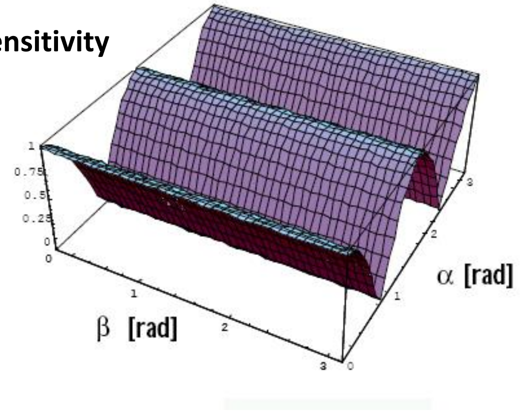

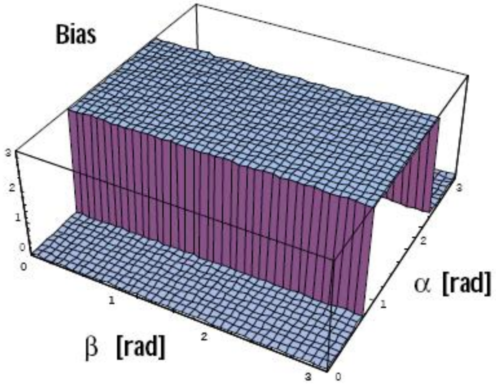

Only birefringence $\boldsymbol{M_s}=\boldsymbol{G}[\delta]$:

$V=1$, $\phi_o=0$

Loop interferometer insensitive on pure birefringence

Not only historical remarks

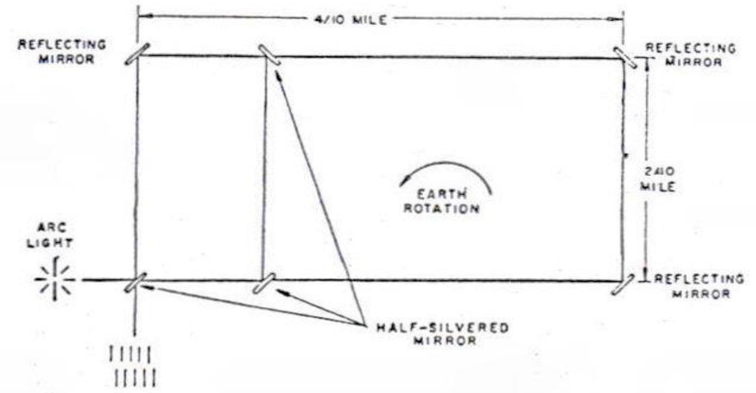

[Post, *Rev. Mod. Phys.*, ***39,*** *1967, 475]*

1904, Michelson loop interferometer (A=834 m^2) for measurement the Earth rotation (1925 with z Henry G. Gale)

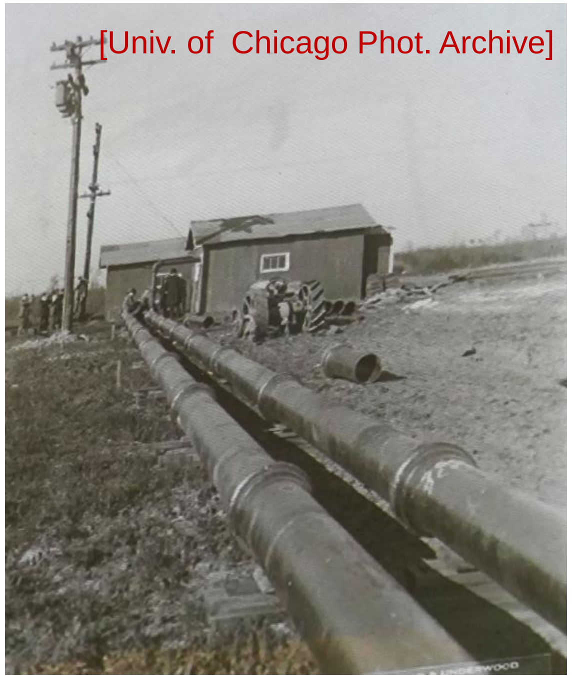

[Univ. of Chicago Phot. Archive]

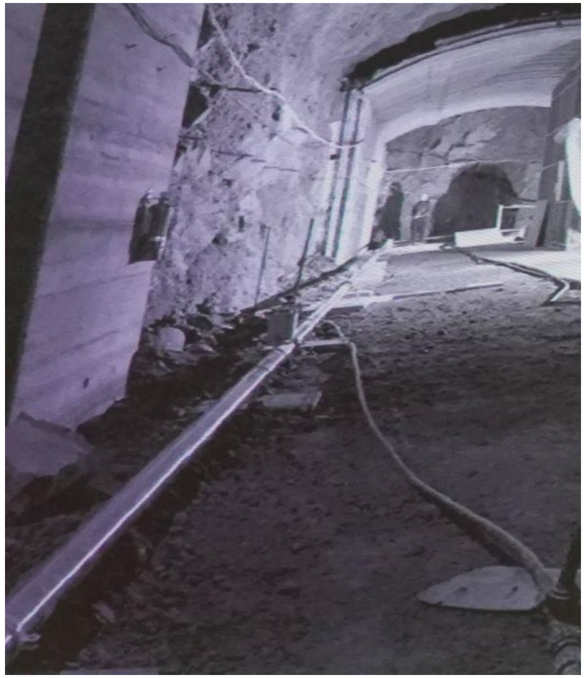

1911 student Harress (by 1914 Herzer), measurement dispersive properties of glasses based on so called Fresnel-Fizeau drag effect.

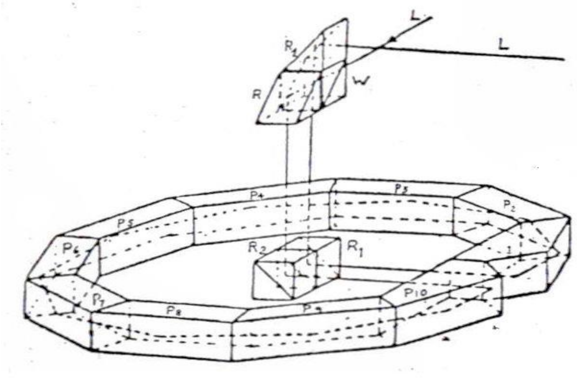

[Post, *Rev. Mod. Phys.*, ***39,*** *1967, 475*]

1911, Max von Laue „Über einen Versuch zur Optik der bewegten Körper”, *Münchener Sitzungsberichte*. 405-412, describing what is today «Sagnac effect», and stating clearly that this effect can be explained classicaly or with Relativity theory.

Sagnac effect

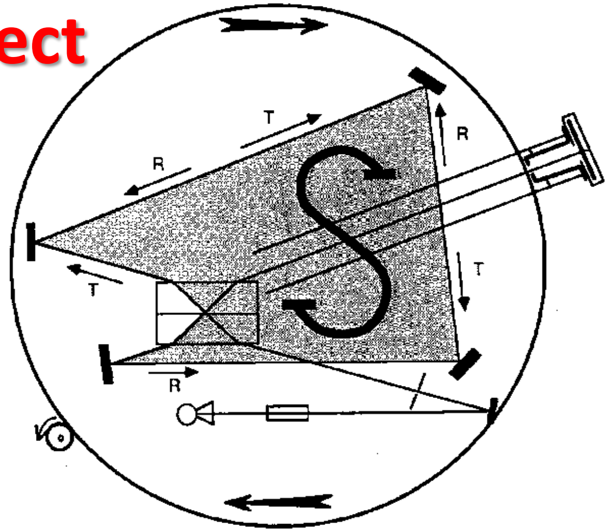

[Post, *Rev. Mod. Phys.*, **39,** 1967, 475]

George Sagnac (1913)/Max Von Laue (1911) effect is a result of a difference between two optical beams propagating around closed optical path, in opposite direction when this path is rotating.

The observed fringes shift is described as:

$$\Delta Z = 4\mathbf{\Omega.S} / \lambda_0 c$$

It is independent of:

- the shape of the surface S,
- the location of the centre of rotation
- the presence of a rotating transparent medium

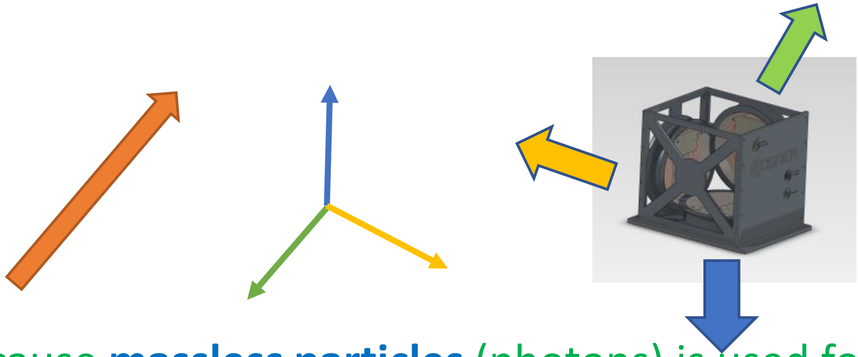

The Sagnac phase shift (1976) induced by rotational rate Ω perpendicular to plane of fiber optic sensor loop is equal to:

$$\Delta\phi = \frac{8\pi A}{\lambda c}\Omega = \frac{2\pi DL}{\lambda c}\Omega = \frac{1}{S_0}\Omega$$

where:
A – optical area
L – length of the fiber in the sensor loop
D– sensor loop diameter
λ – wavelength
c – velocity of the light in vacuum
S_0 – the optical constant of interferometer

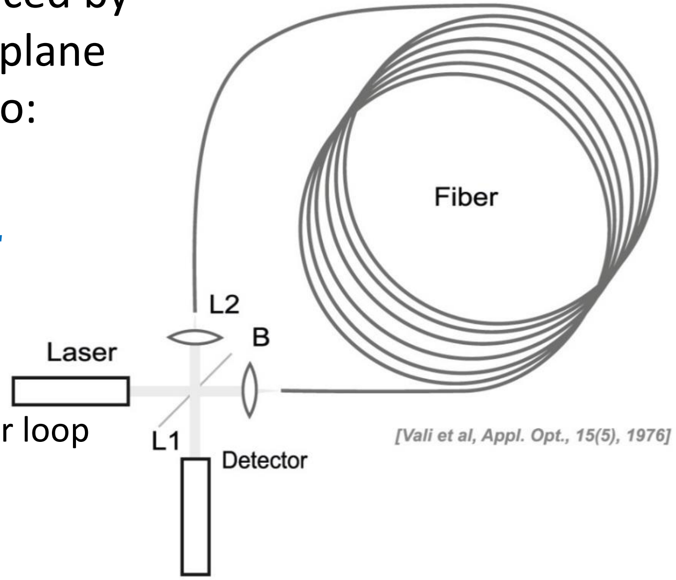

[Vali et al, Appl. Opt., 15(5), 1976]

- Because **massless particles** (photons) is used for the measurement, device is entirely **insensitive to linear accelerations, no-exist cross coupling** as well as it has **BB flat response**,
- There is **no moving part** except photons, which allows **maintenance free** and **small environment sensitivity**

Fiber Optical Gyroscope

Ring Laser Gyro - RLG

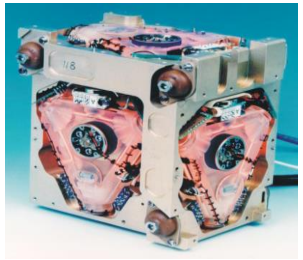

- Resonant ring of 10 to 30 cm perimeter.
- He-Ne plasma laser with high-voltage discharge.
- Very simple read-out signal: frequency beating.
- Dead zone about zero solved with mechanical "dither" (two 500 THz oscillators with 1 Hz difference for 1 deg/h!)
- By the way, an amusing coincidence: 400 nm and 750 nm correspond to 700 THz and 400 THz
- Improved lifetime (5 to 7 years operating) compared to mechanical gyros, but still limited: wearing-out electrodes and helium leakage

Fiber-Optic Gyro - FOG

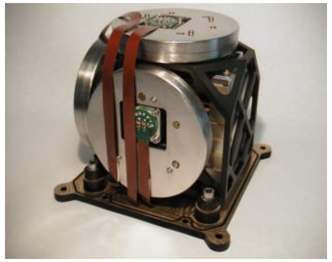

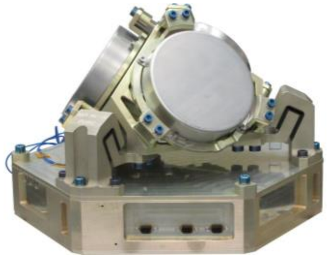

- Ring interferometer with a fiber coil (100 m to 10 km over 3 to 30 cm, i.e. 0.7 to 700 m^2).
- Fully solid-state components derived from optical-fiber communication components: low-attenuation single-mode optical fiber, but also, laser diode, erbium-doped-amplifying fiber, integrated optic circuit, fiber components (coupler, isolator, circulator, Bragg grating…)
- Much longer lifetime.
- Low power, low voltage.
- No acoustic noise.

IMU Grade	Main paremeters		
	ARW (white noise)	**Bias Drift**	**SF accuracy**
	[(°/h)/$\sqrt{Hz}$]	[°/h]	[ppm]
Rate	> 0.5	1 000 - 10	10^4 -10^3
Tactical	0.5 - 0.05	10 - 1	1 000 - 100
Intermediate	0.05 - 0.005	1 - 0.01	100 - 1
Inertial	0.005 - 0.0003	0.01 - 0.001	5
Strategic	< 0.0003	< 0.001	1

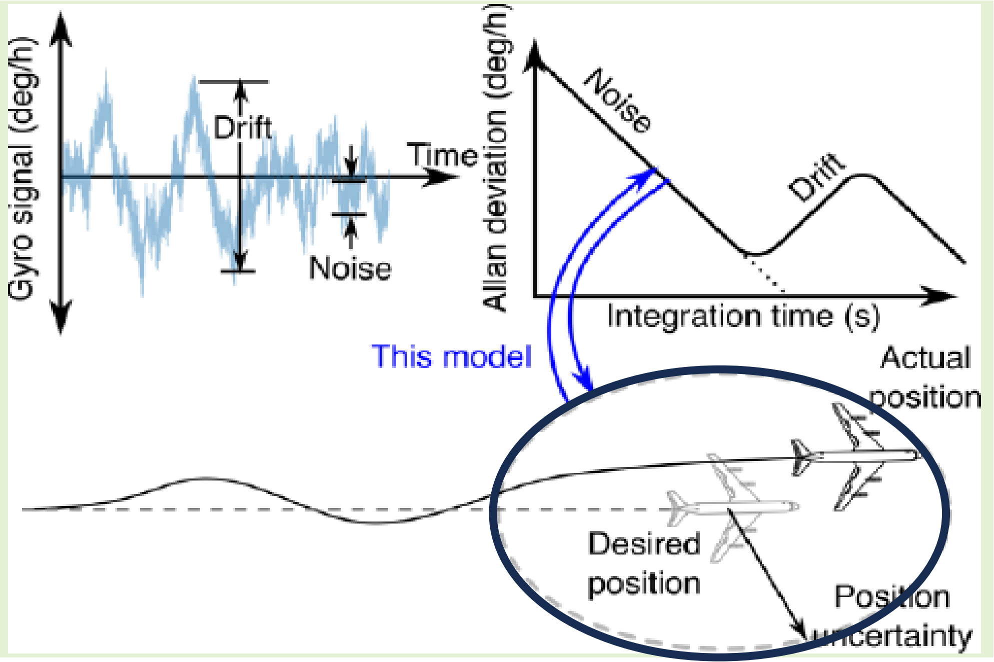

Based on lecture H. LeFavre, EWOFS-5 Kraków, 2013

1 [deg/h] ~5.10^{-6} [rad/s]
0.01 [deg/h] for intermediate 10^{-8} [rad/s]

FOG's devil

10^{-8} [rad/s] => ? $\Delta L = \frac{\lambda}{2\pi}\Delta\phi \;=\frac{LD}{c}\Omega = \frac{1\,000[m]*0.1[m]}{3\;10^{8}[m/s]}10^{-8}\left[\frac{rad}{s}\right] = 3\;10^{-15}[m]$

The range od hydrogen nuclei diameter !!!!

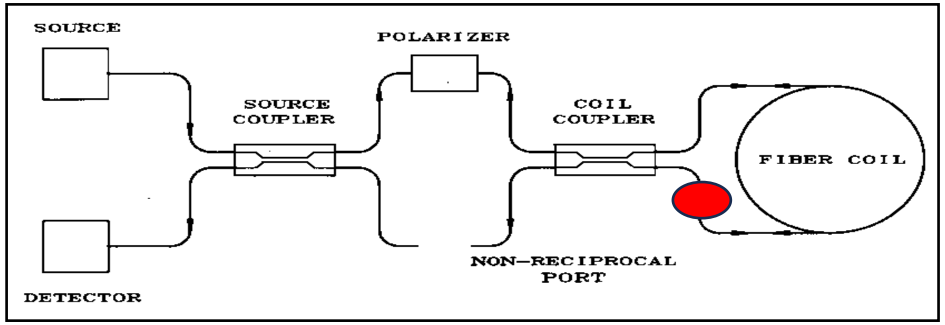

[Urlich, 1980, Arditty & Lefevre, 1981]

RLG
Giant > 10 m^2

Scalability of the Area
[A=(LD)/4}

FOG
Large ~1 000 m^2

Increase the numer of turns

Increase the area of each turn

Finesse is limited by mirror quality, gain, output optical power…
Square design => limited benefit
Perimeter longer than 30 cm => harder longitudal monomode

Optical fiber attenuation leads to a finite optimal length beams propagating
Winding capability limit
Homogenous environment harder to achieve for large coil

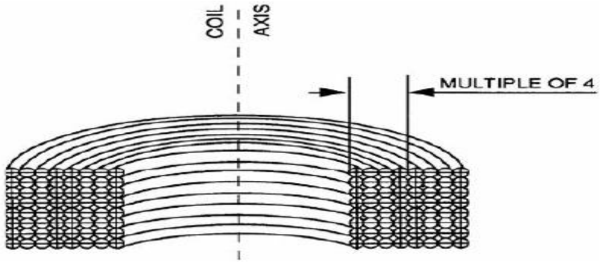

$$\Omega_{min} = \frac{\lambda c}{\sqrt{2}\pi DL}\sqrt{\frac{4kT}{R*\eta^2*\left(P*10^{-\left[a+b\frac{L}{1000}\right]/10}\right)^2} + \frac{eI_D}{\eta^2*\left(P*10^{-\left[a+b\frac{L}{1000}\right]/10}\right)^2} + \frac{e}{\eta*P*10^{-\left[a+b\frac{L}{1000}\right]/10}} + \frac{\lambda^2}{4c\Delta\lambda}} = \frac{\sqrt{2}\lambda c}{2\pi DL}\sqrt{N_T + N_D + N_P cos^2\left(\frac{\phi_b}{2}\right) + RIN\left(\frac{1+cos\phi_b}{1+cos(\pi/2)}\right)^2}$$

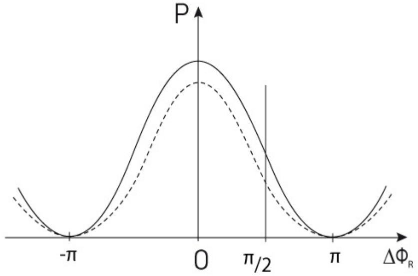

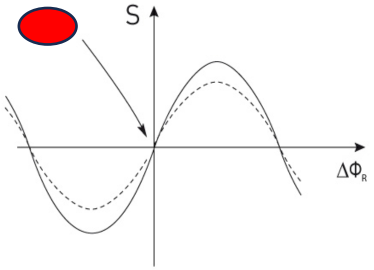

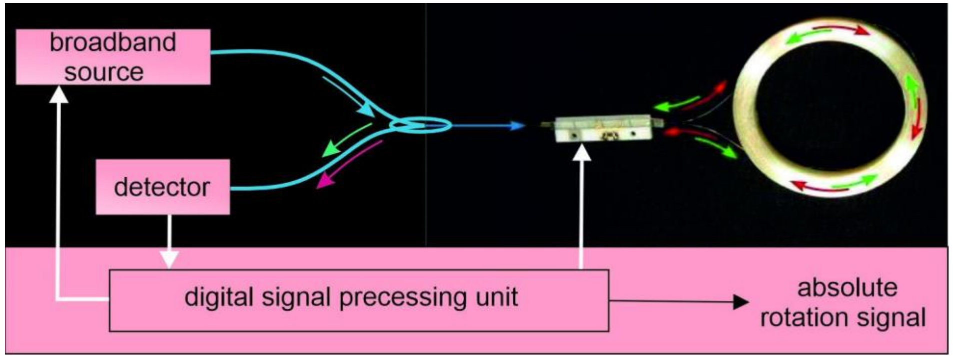

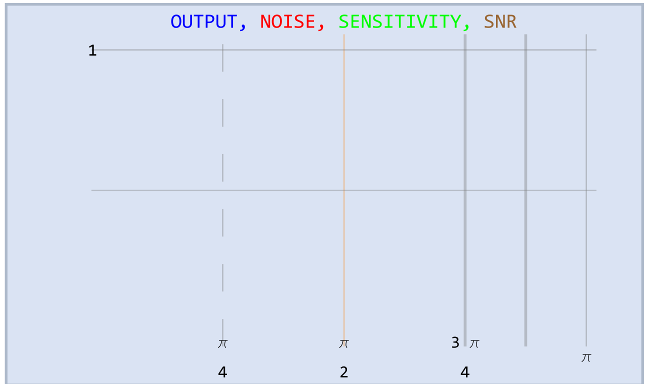

The baby out with the bathwater

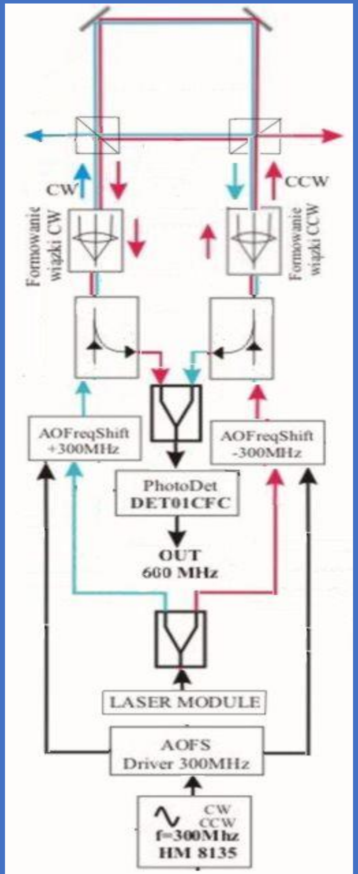

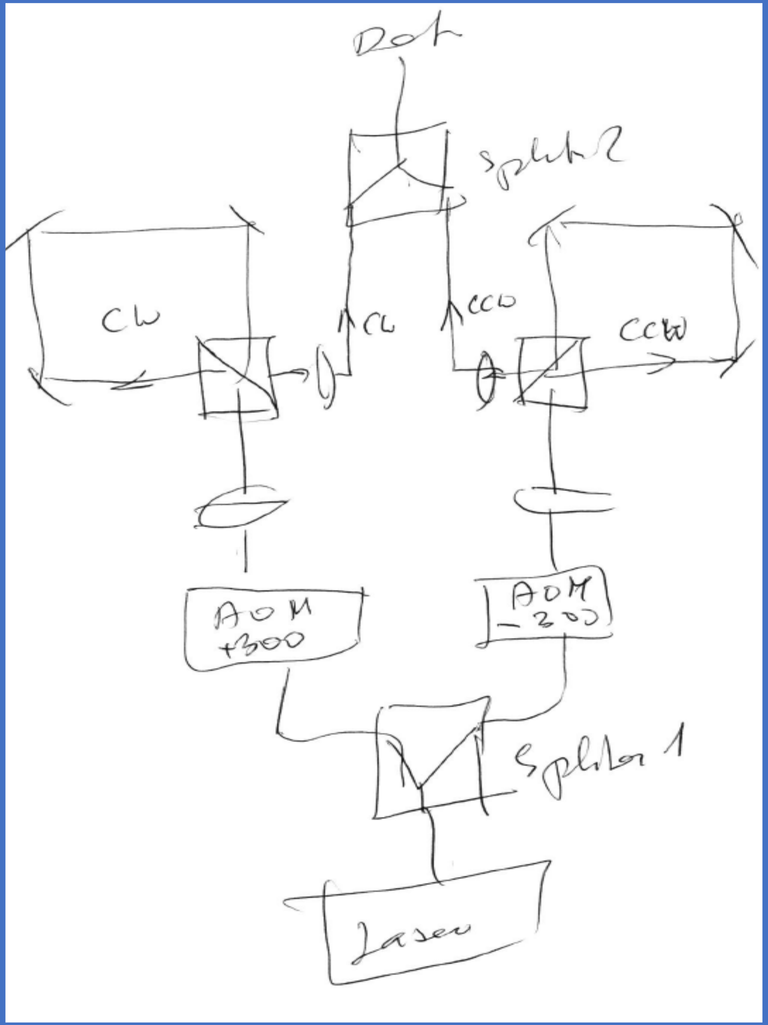

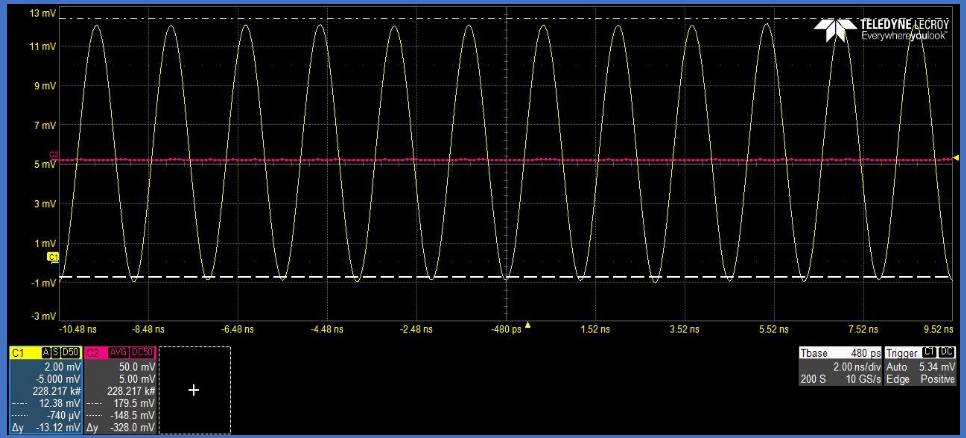

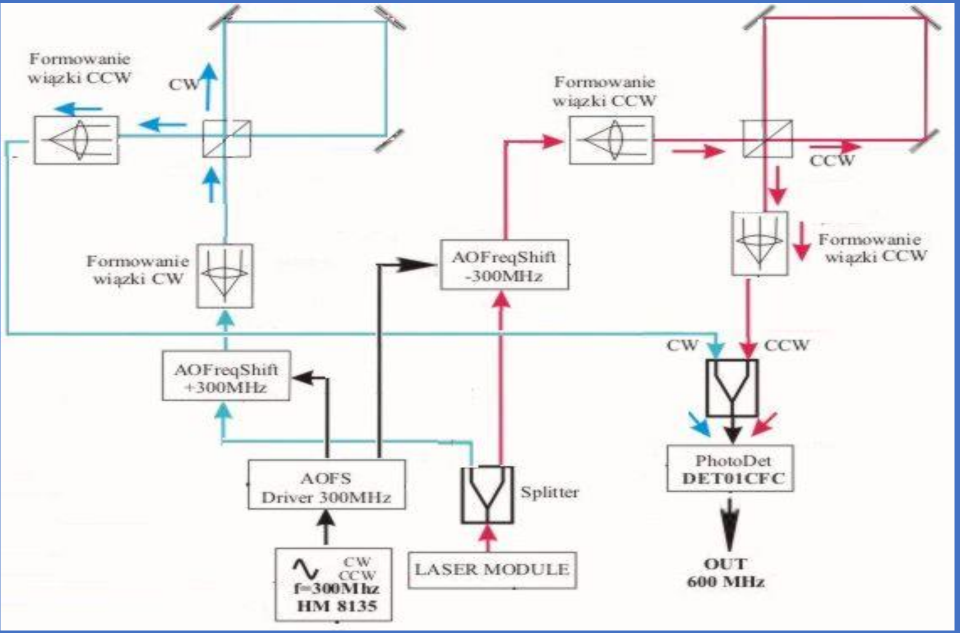

Rotational Seismometer - FOG's devil with wings

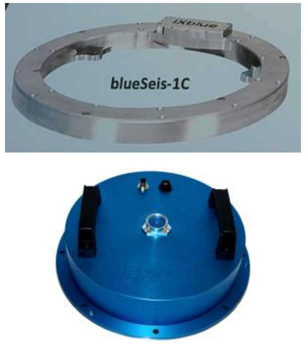

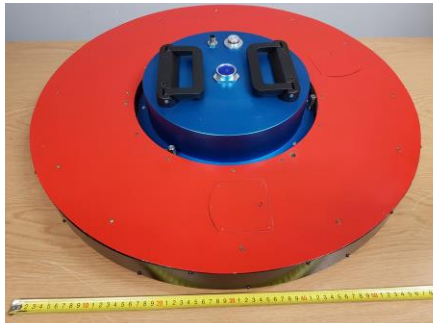

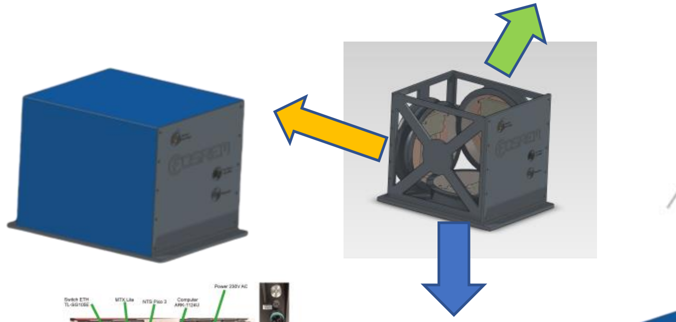

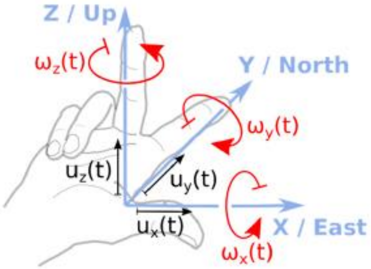

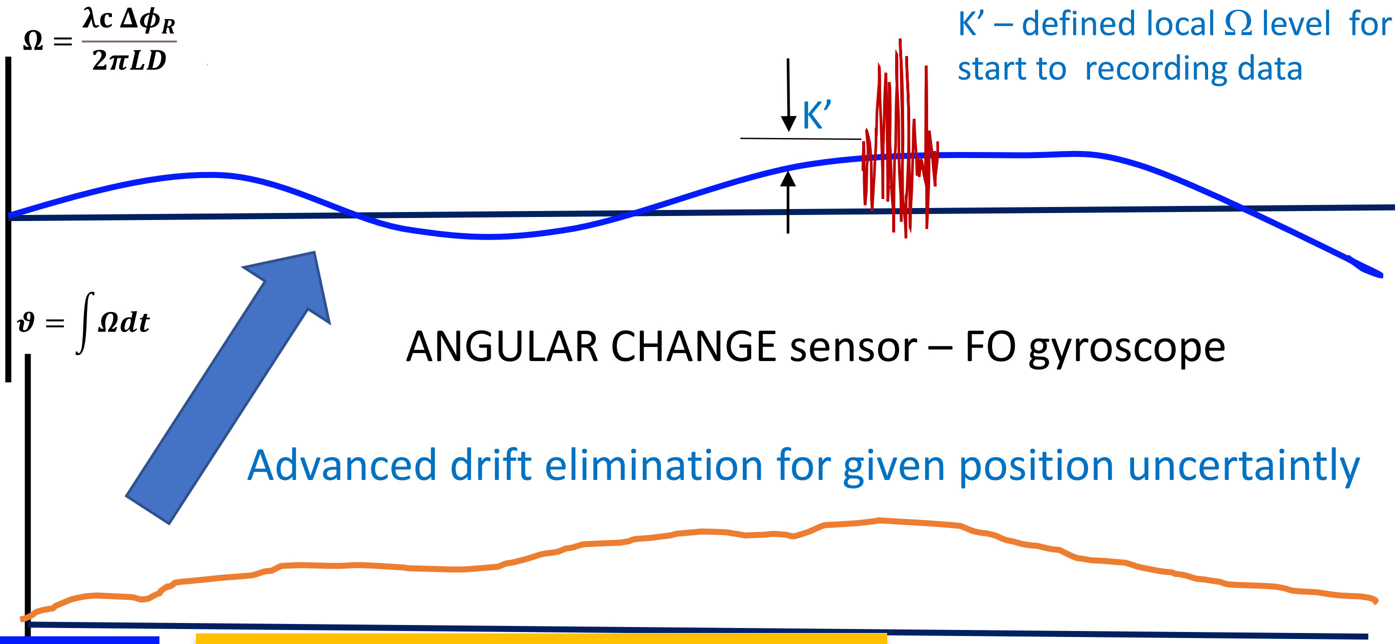

Seismological application

signal amplitude:
from 10^{-8} rad/s,
frequency:
0.01 Hz – 0.1 Hz

[Bernauer et al., *J. Seismol.*, **16**, 2012, 595]

Common

- insensitivity to linear motion, or
- opportunity to detect linear and rotational motions independently,
- mobility,
- stability with respect to environmental conditions, including changes of temperature,
- independent power supply,
- power consumption 5 – 8 W

Engineering application

signal amplitude:
up to a few rad/s,
frequency:
0.01 Hz – 100 Hz

[Jaroszewicz et al., *Sensors*, **16**, 2016, 2161]

ROTATIONAL SEISMOGRAPH
set of RSs + precise time source + recording device + network

[Havskov et al. *Instrumentation in Earthquake Seismology.* Springer, 2016]

Real examples

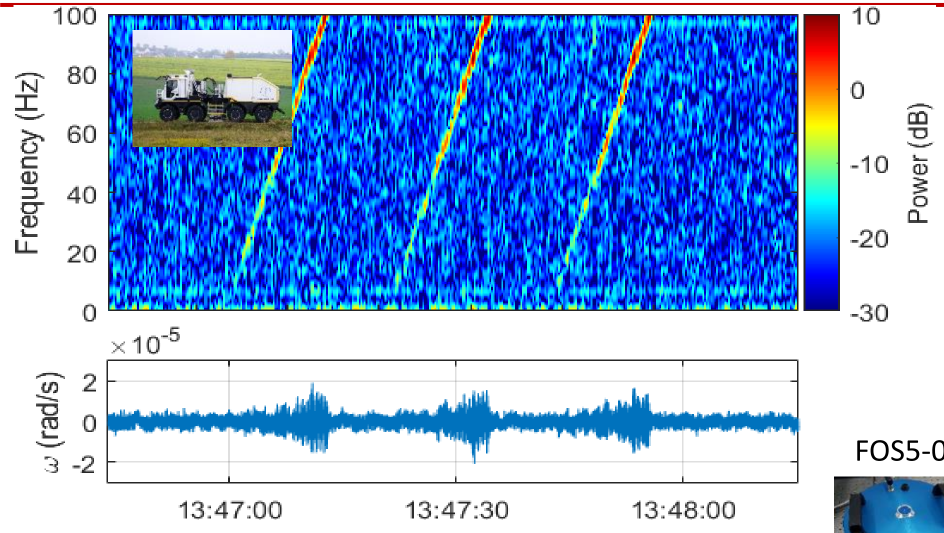

[Kurzych et al., *Opto-Elect. Rev*, **29**, 2021, 39]

FOS5-02

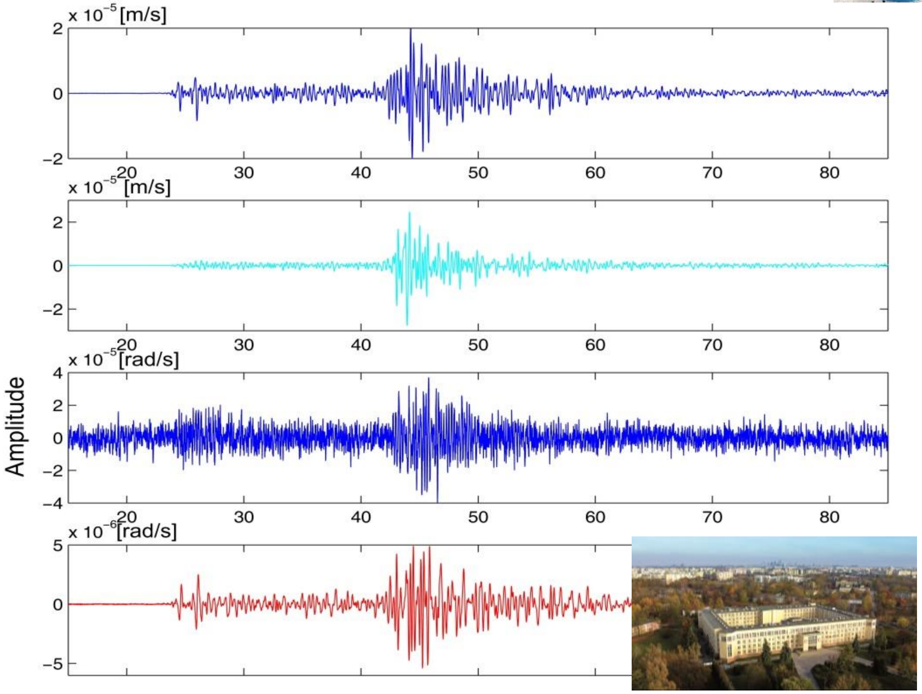

[Kurzych et al., *Opto-Elect. Rev*, **28** 2020) 69]

Coalmine "Ignacy" in Rybnik

Książ Castle

- touristic activity
- changes of Earth's rotation rate due to diurnal polar motions, as well as diurnal and semidiurnal tides.

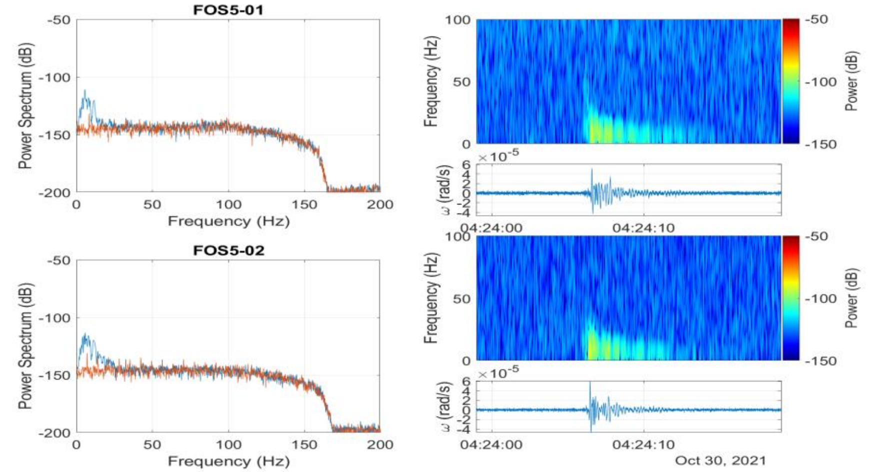

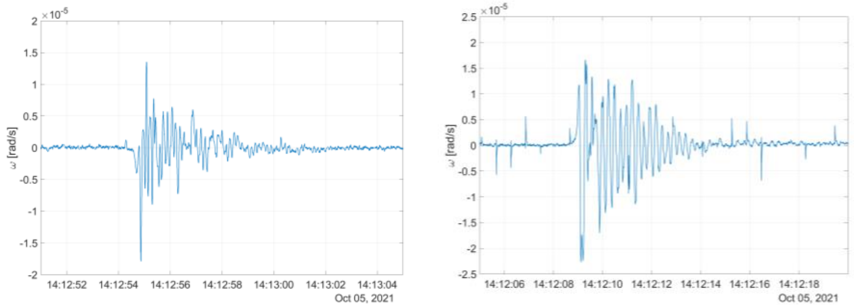

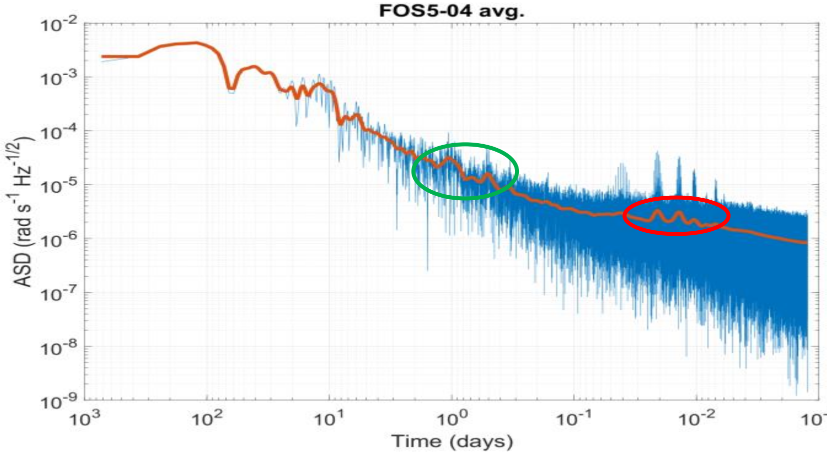

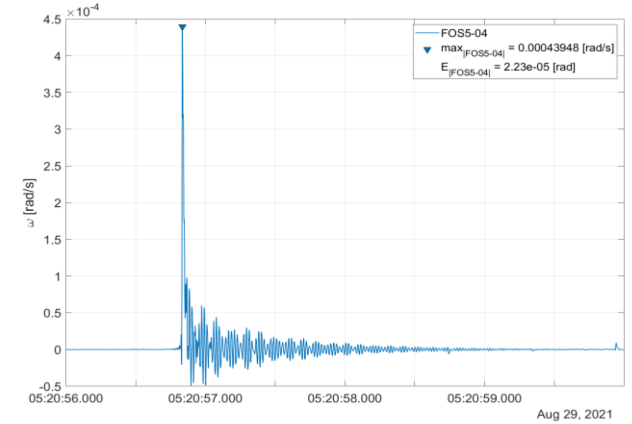

[Jaroszewicz et al., *Opto-Elect. Rev*, **29**, 2021, 213]

IWGoRS test in November 2019 Furstenfeldbruck, Germany

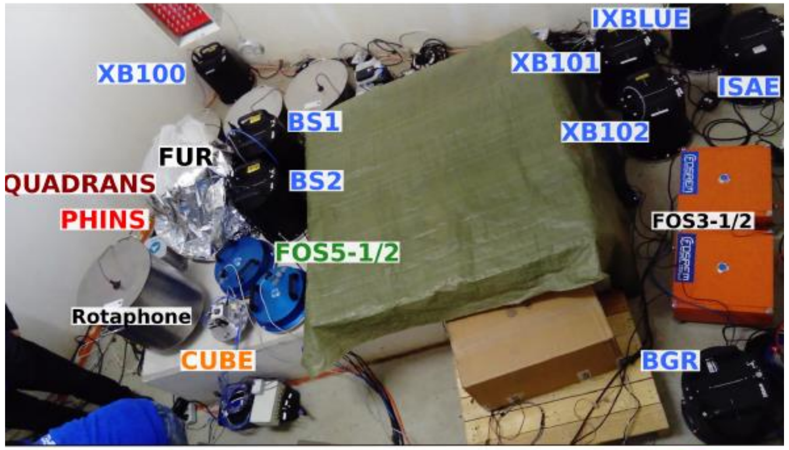

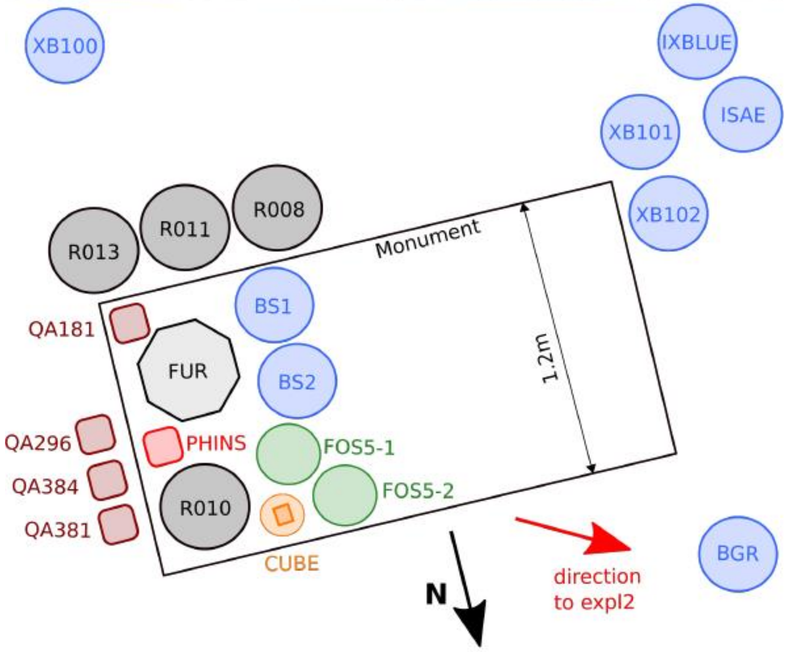

[Bernauer et al., *Sensors*, **21,** 2021, 264]

More than 24 different sensors:

- bb Seismometer
- ROMY
- blueSeis-3A - eight
- FOS3 – two
- FOS5 - two
- Rotaphone
- Phins - one
- Quadrans - four
- Cube – four HORIZON
- Geophone
- DAS

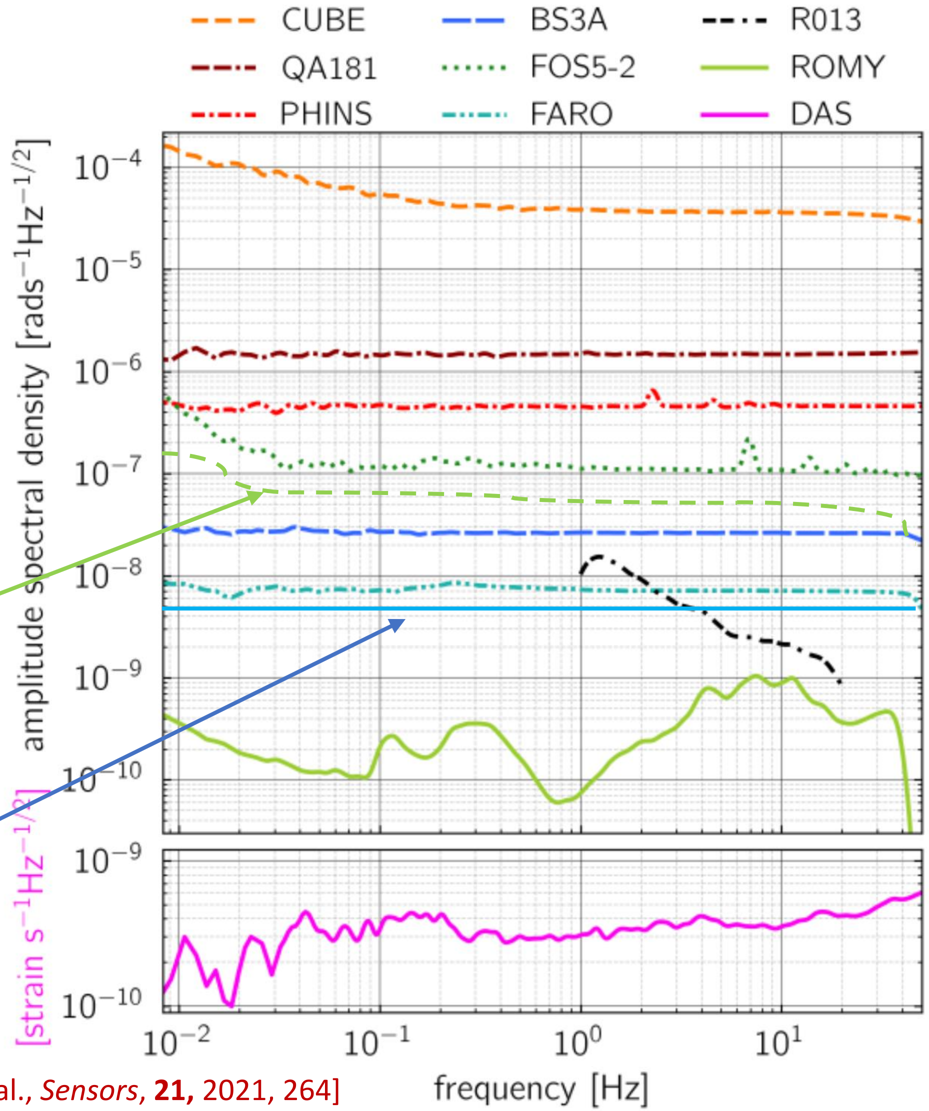

[Bernauer et al., *Sensors*, **21,** 2021, 264]

Waveform coherency during huddle test

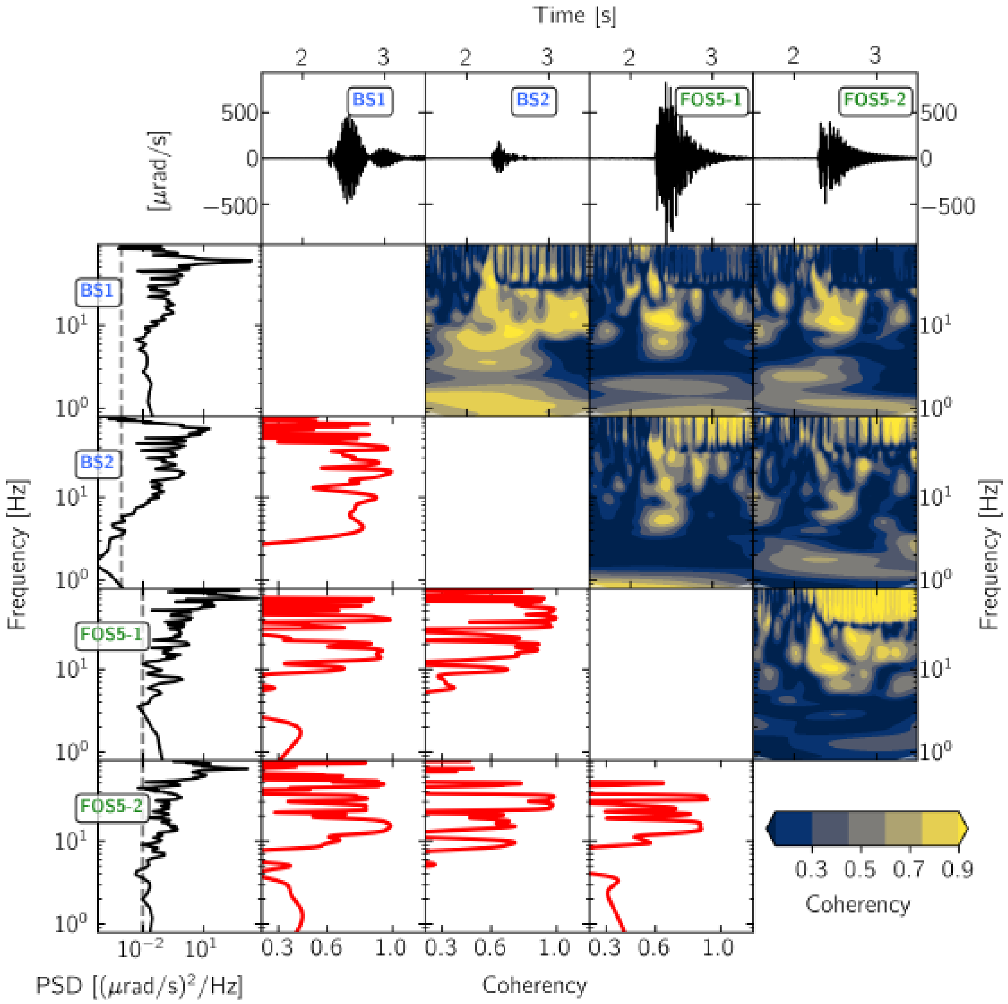

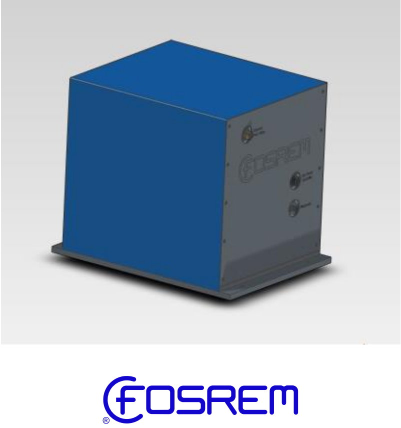

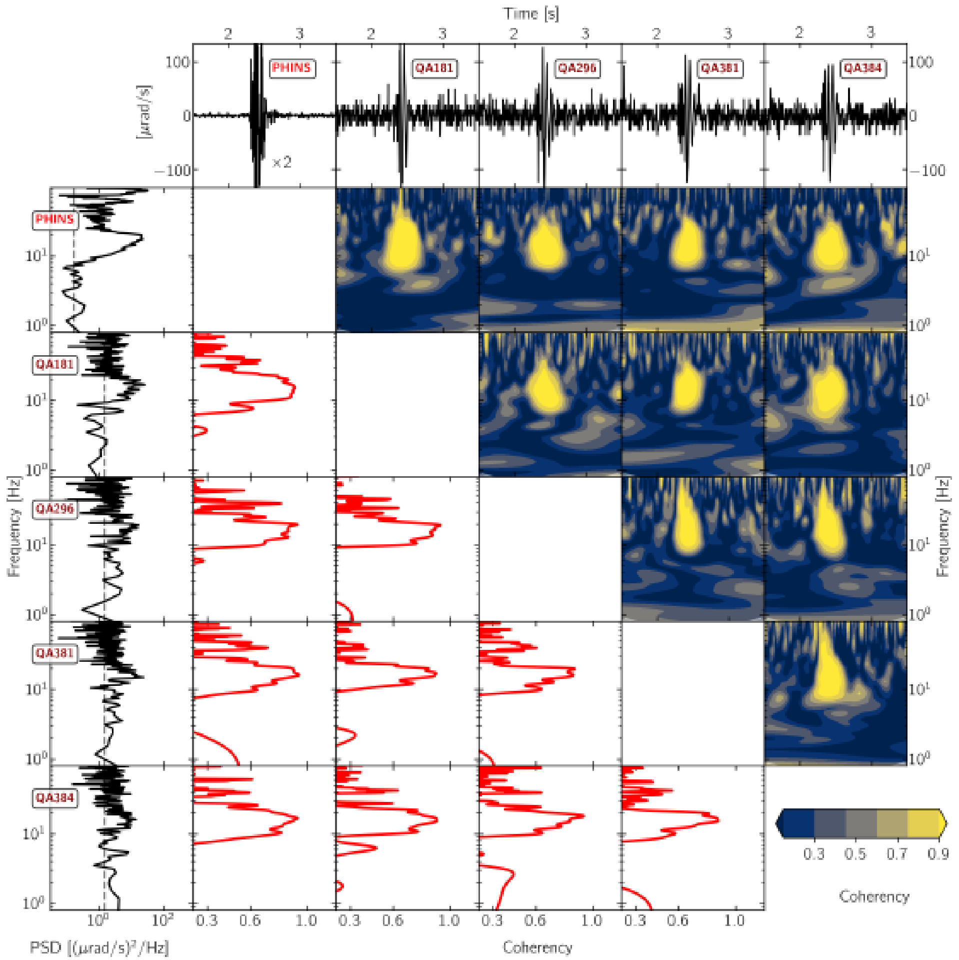

[Bernauer et al., *Sensors*, **21,** 2021, 264]

A high level of coherency and waveform similarity within a narrow frequency range (10 Hz - 20 Hz) for recordings from a nearby explosion signal

Perimeter security system

- Major source of phase error in FOG may occur if rapid changes in optical path length, due to thermal or mechanical effects on the fibers, because the cw and ccw beams encounter the temporally varying path length changes at different moments in time and therefore will suffer **different phase changes**!!!

The $d\Phi/dt$ is not readily measured directly, but by incorporating an additional optical fiber path from the source, together with the path taken by one of the counter-propagating beams from the Sagnac loop, a MZI my be formed.

The MZI gives output proportional to Φ and differentiation yields to required $d\Phi/dt$. Simple division of the Sagnac phase offset by $d\Phi/dt$ finally gives the desired distance Z, of point of disturbance P:

1. rate of change $d\Phi/dt$, of the optical signal, induced at the point P, by external influence,
2. distance Z between point P and the coil centre 0

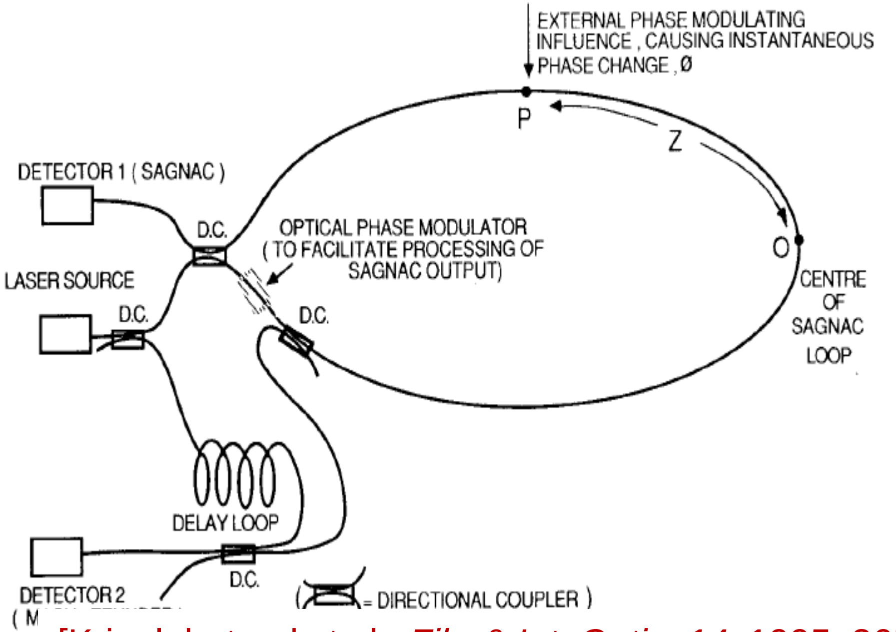

[Kringlebotned et al., *Fib. & Int. Optic*, *14*, 1995, 365]

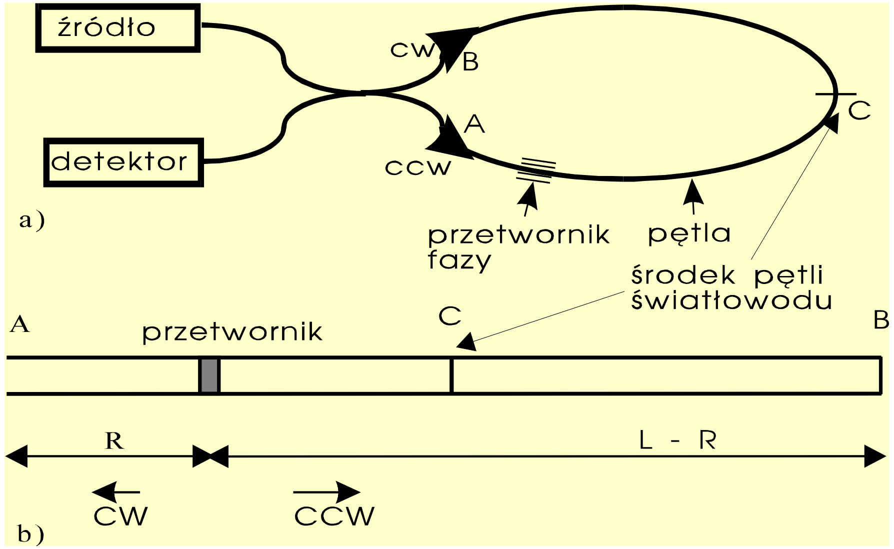

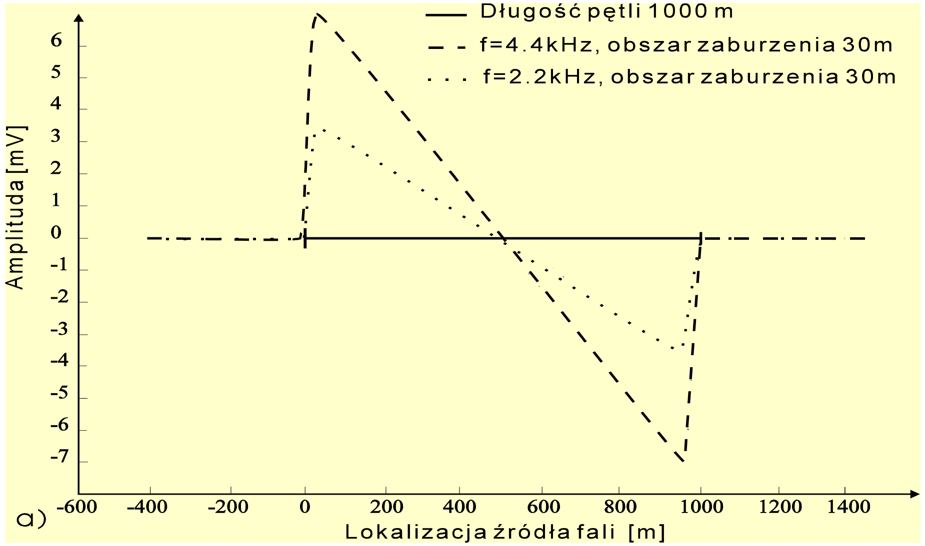

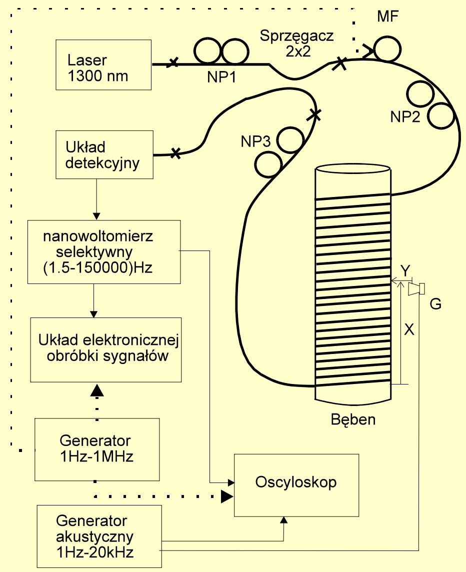

a)

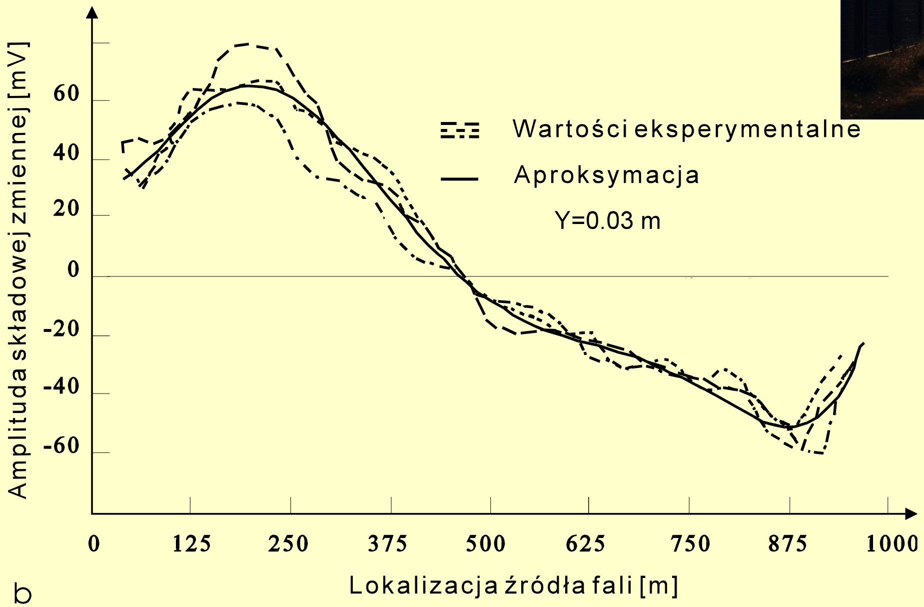

b

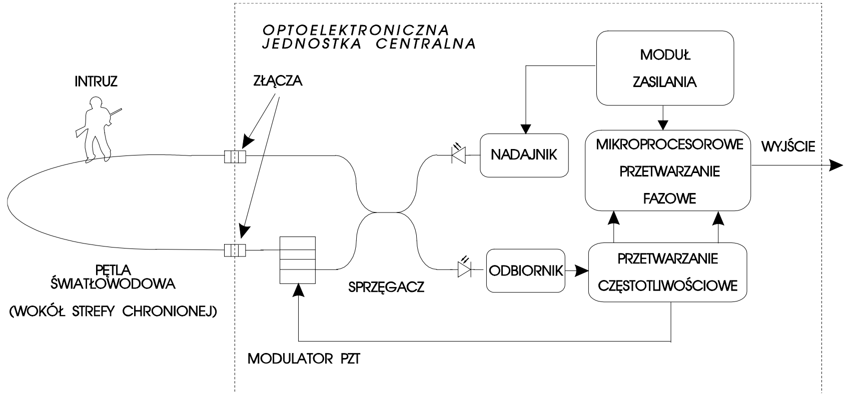

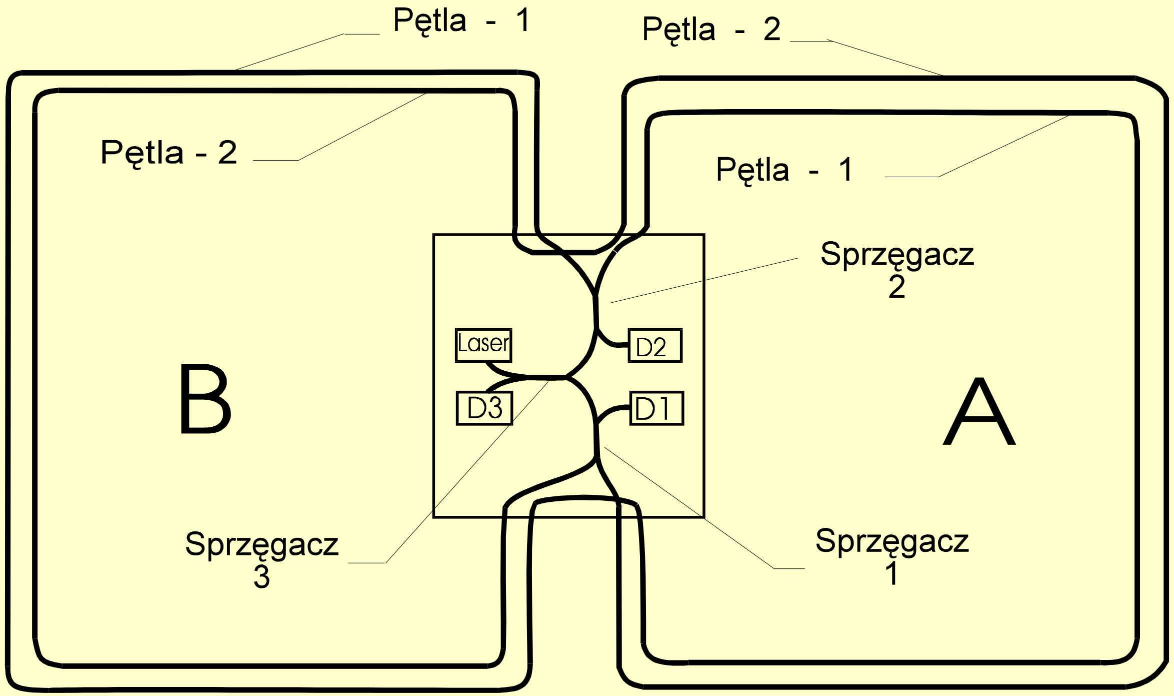

[Jaroszewicz et al., *Proc SPIE*, ***2341***, *1994*, *84*]

FOIPA - FO Interferometric Polarisation Analyzer

The system operation is birefringence modulation in a SMF followed by suitable detection amplitudes of first three tones from output electronic signals and based on them identification polarization parameters.

$$\Delta = \arctan(\alpha),\quad \phi = \tfrac{1}{2}\arctan(\beta/\gamma),\quad P=\sqrt{\beta^2+\gamma^2}$$

$$\alpha = \frac{J_2(\delta_0)U2_\omega}{J_1(\delta_0)U2_{2\omega}},\quad \beta=\frac{U1_{2\omega}}{2U_{01}J_2(\delta_0)},\quad \gamma=\frac{1}{2U_{02}}\sqrt{\left(\frac{U2_\omega}{J_1(\delta_0)}\right)^2+\left(\frac{U2_{2\omega}}{J_2(\delta_0)}\right)^2}$$

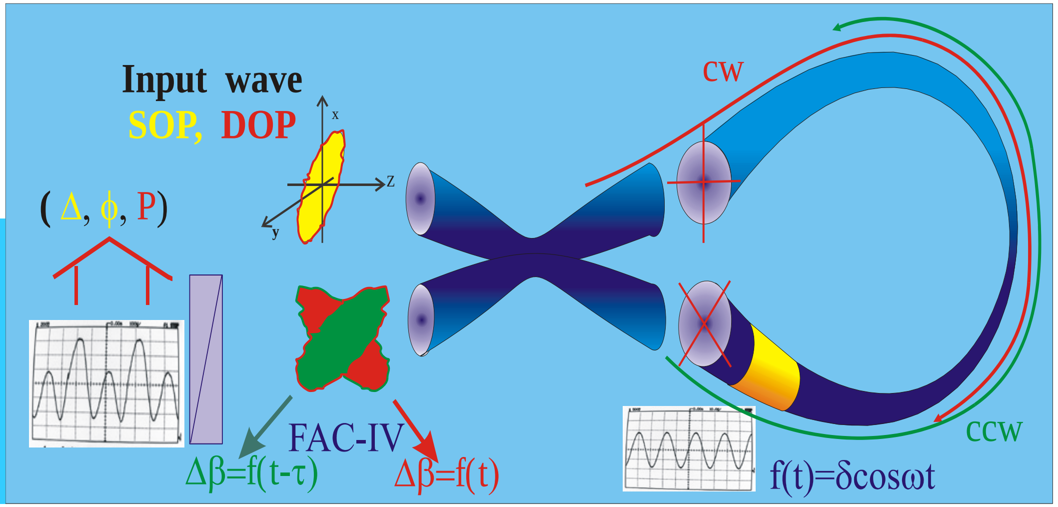

The system require fulfillment IV-th Fresnel-Argo interference condition (interaction of two orthonormal polarized beams).

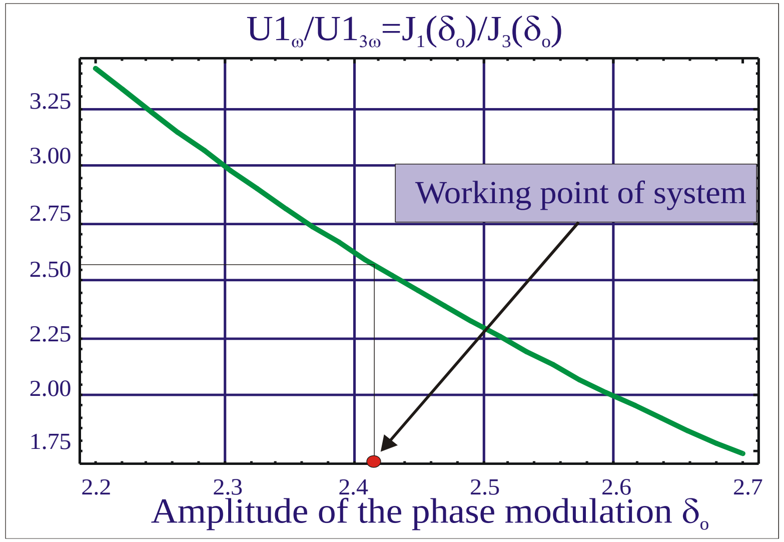

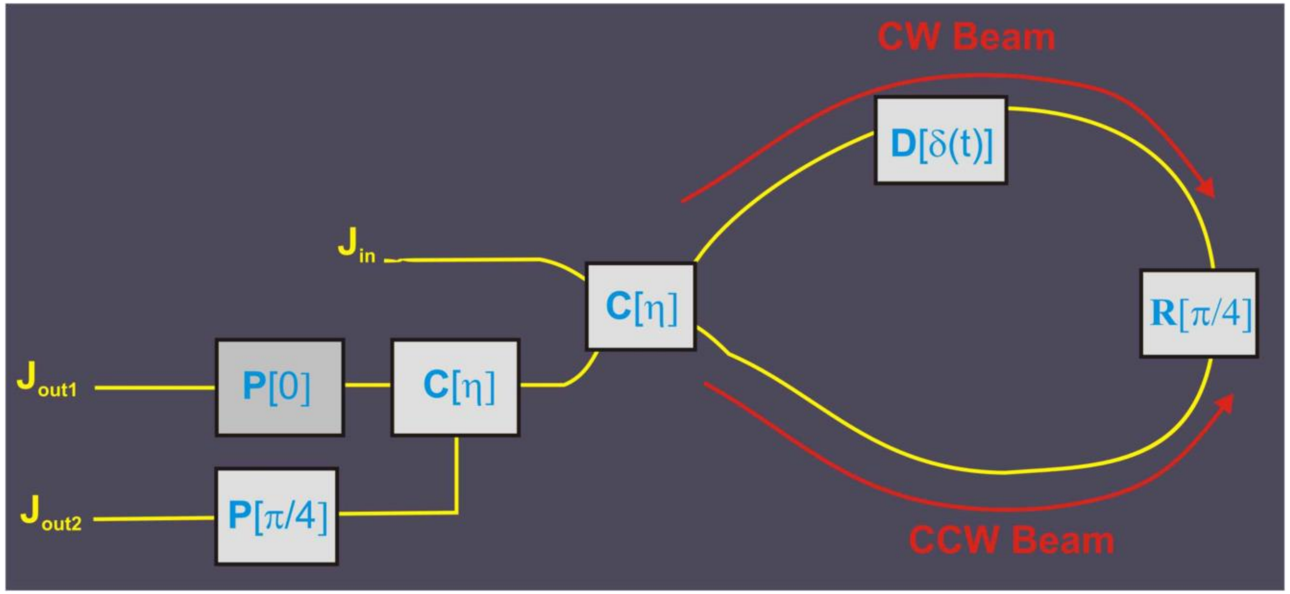

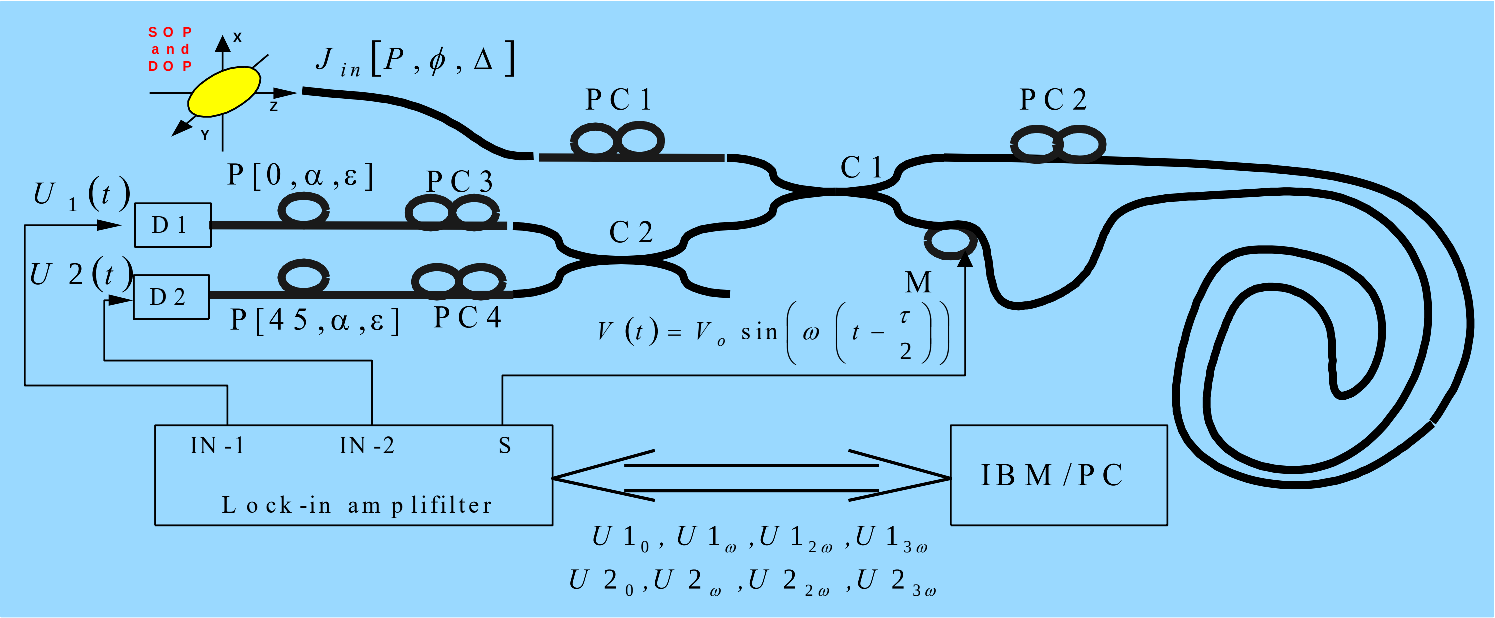

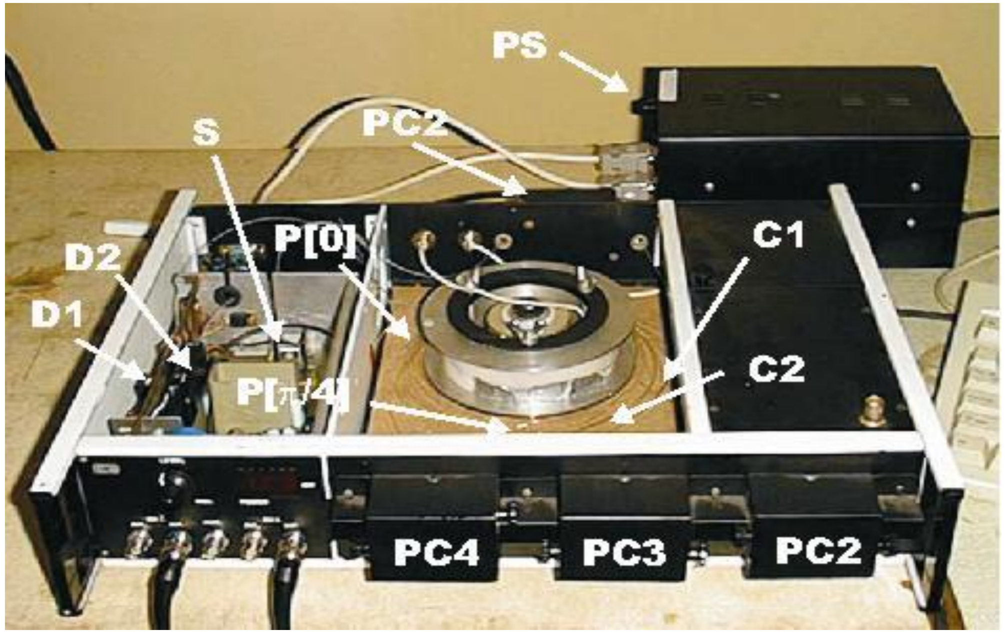

[Jaroszewicz et al., *IEEE Sensor J.*, **3**, 2003]

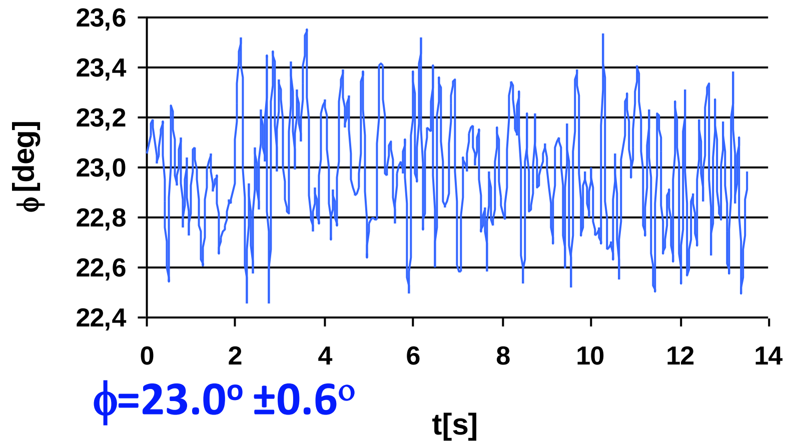

$\phi=23.0^o \pm 0.6^o$

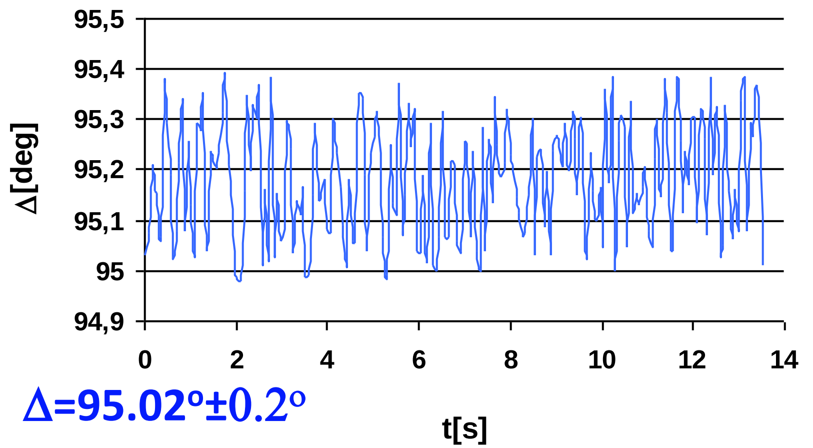

$\Delta=95.02^o \pm 0.2^o$

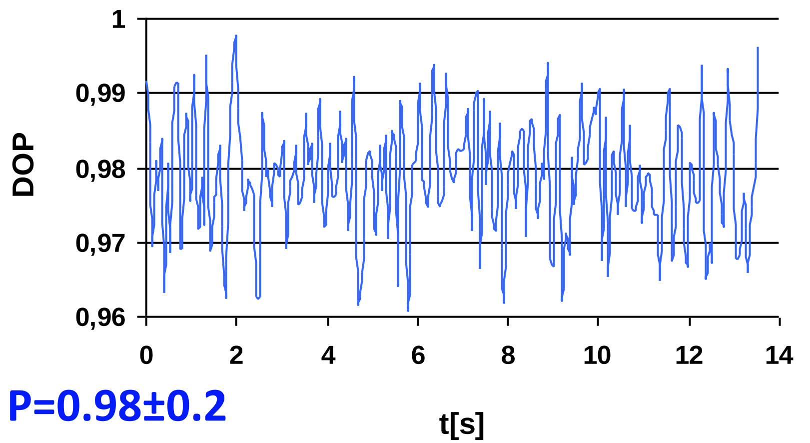

P=0.98±0.2

FLM – Fiber Loop Mirror

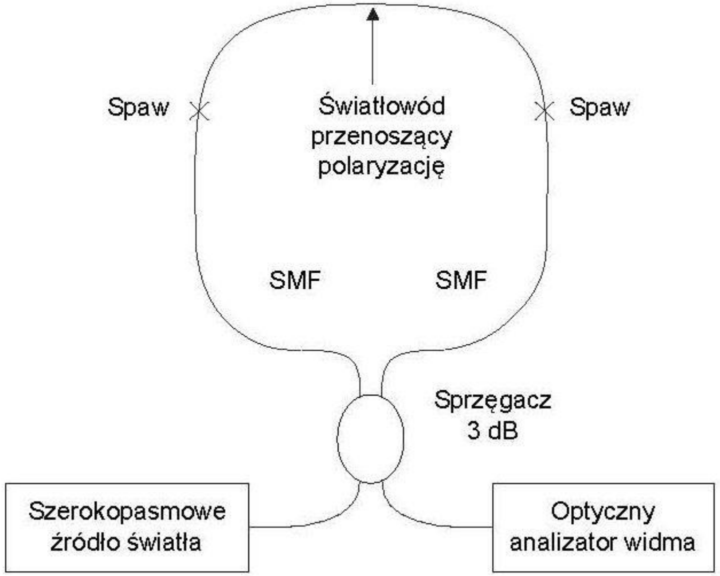

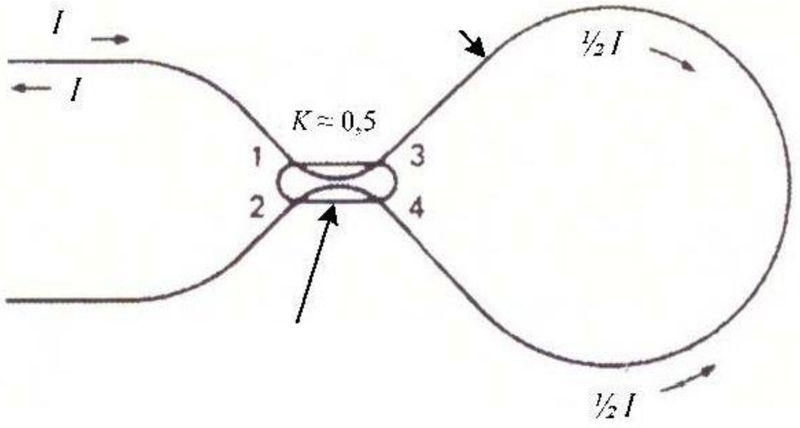

[Mortimore, *JLT*, **6**, 1988, 1217]

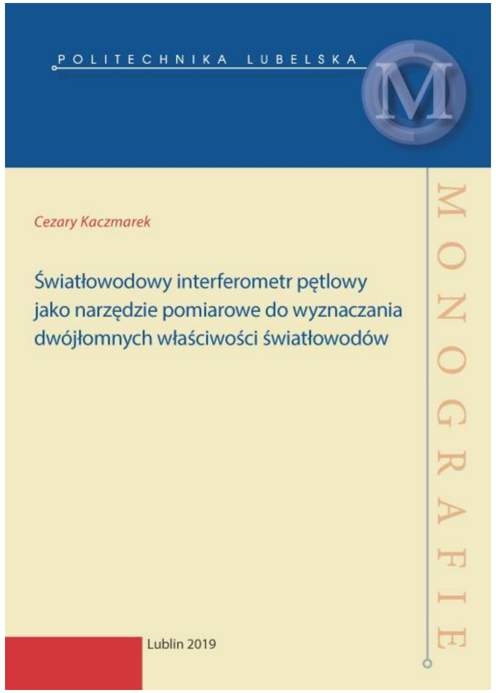

Transfer function:

$$T = \frac{1}{2}[1 - \cos\Delta\varphi] \quad \Delta\varphi = \varphi_x - \varphi_y = \frac{2\pi L \Delta n}{\lambda}$$

1. group birefringence is obtained from period of spectral oscillation

$$\frac{d\Delta\varphi}{d\lambda} = \frac{2\pi L}{\lambda^2}(-\Delta n_G) =>_{|\Delta\varphi=2\pi} \; \Lambda = \frac{\lambda^2}{L\Delta n_G}$$

2. external factor X interaction with FLM

$$\frac{d\Delta\varphi}{dX} = \frac{2\pi}{\lambda}\left(L\frac{\partial\Delta n}{\partial X}dX + \Delta n\frac{\partial L}{\partial X}dX\right)$$

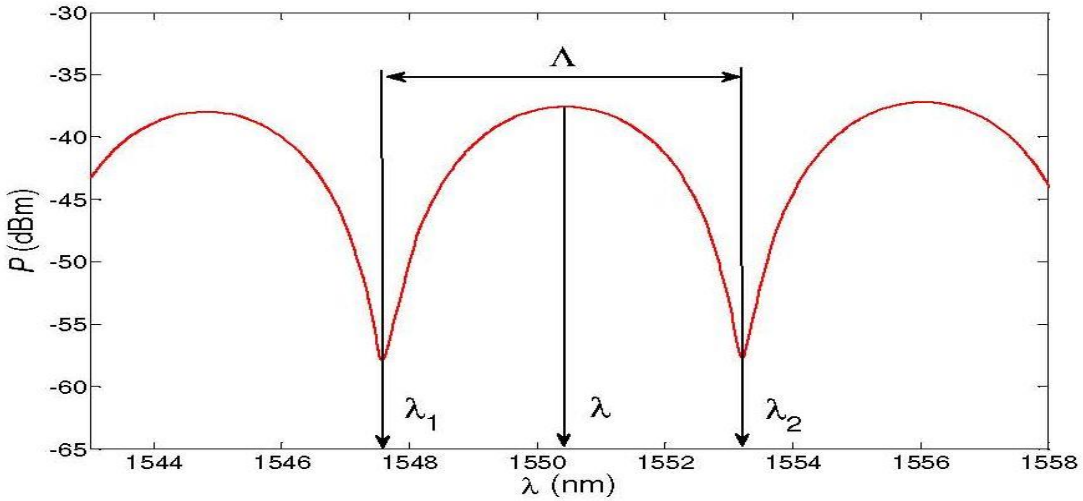

Phase & group birefringence

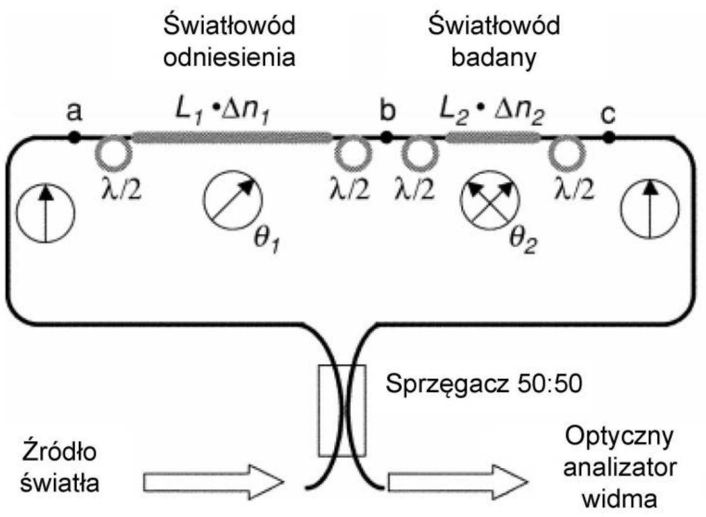

$$\Lambda_{s,L} = \frac{\lambda^2}{\Delta n_1 L_1 \pm \Delta n_2 L_2}$$

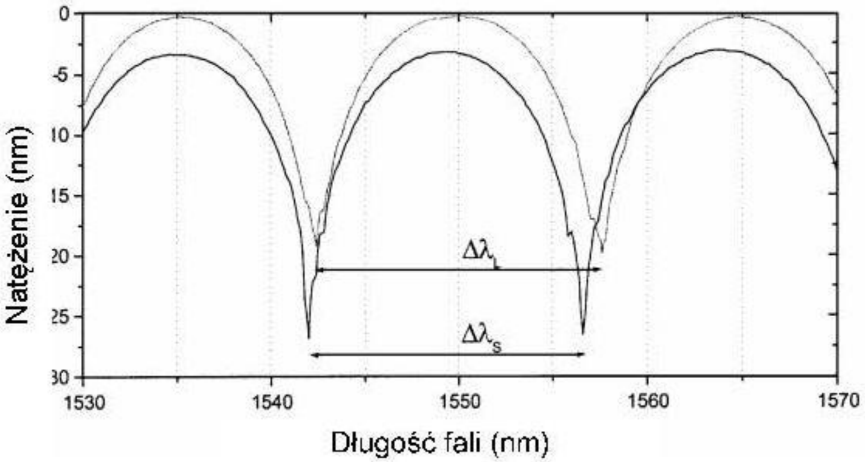

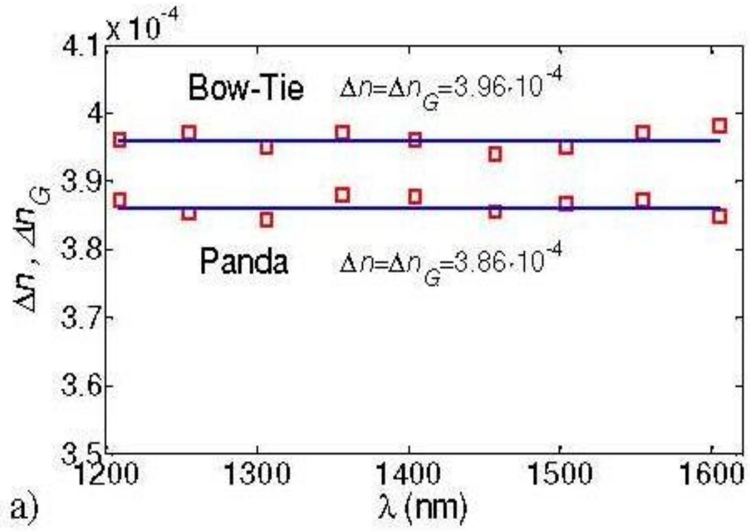

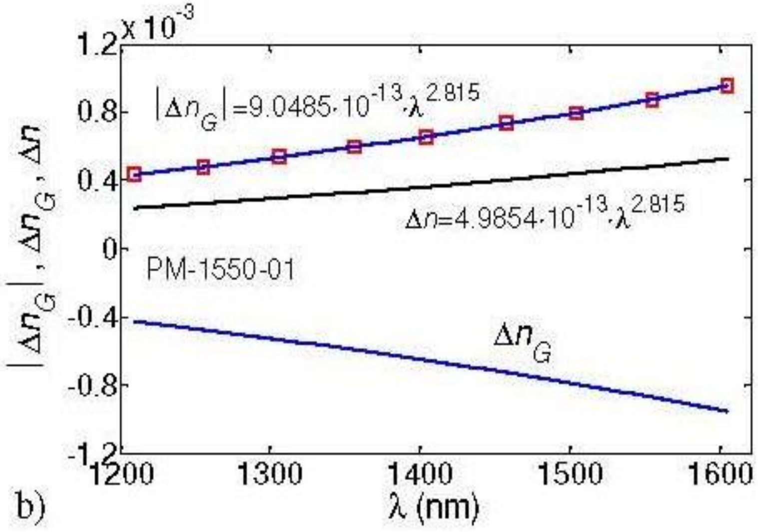

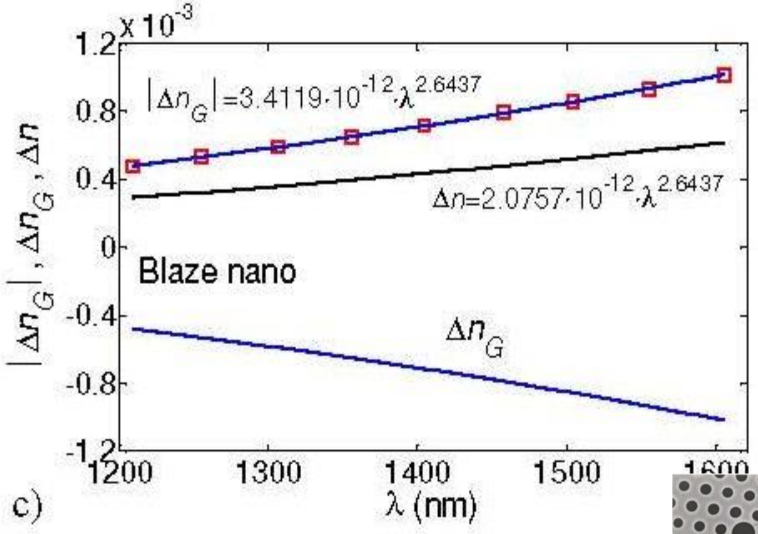

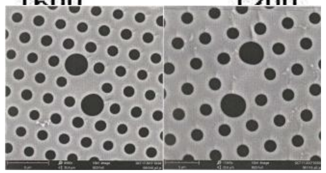

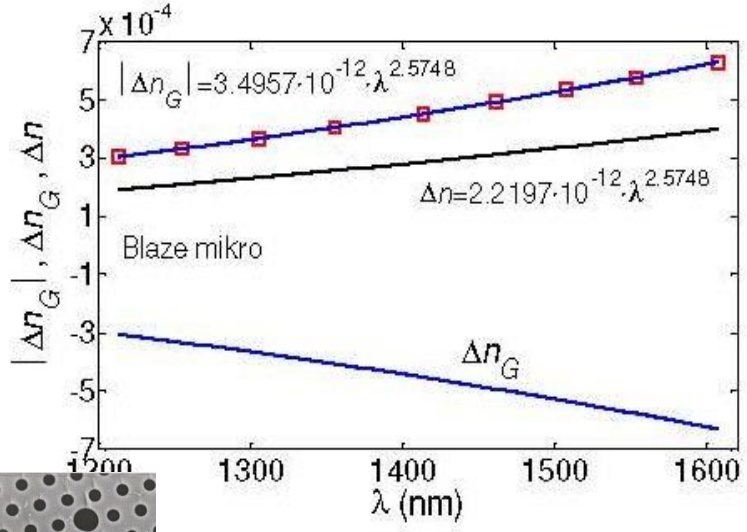

Modal birefringence sensitivity

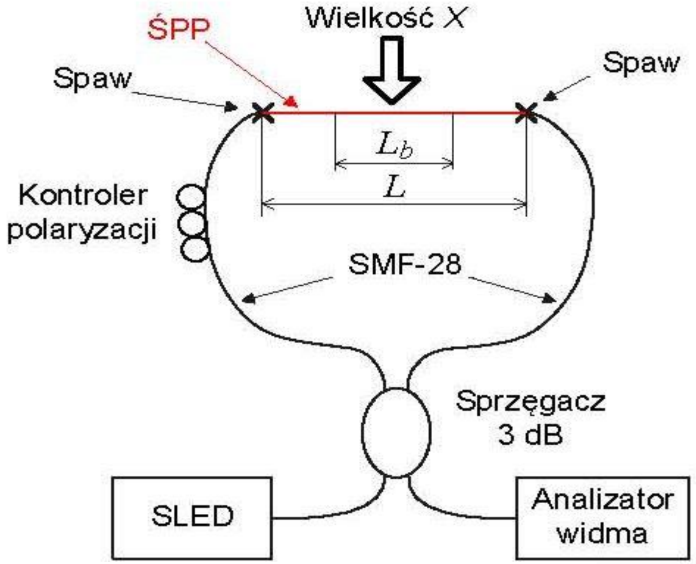

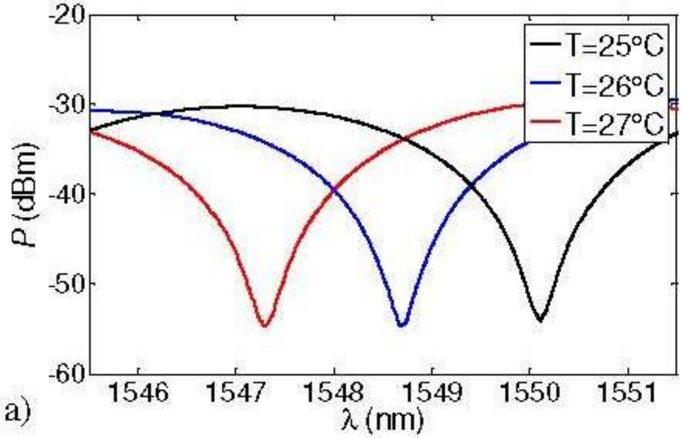

a)

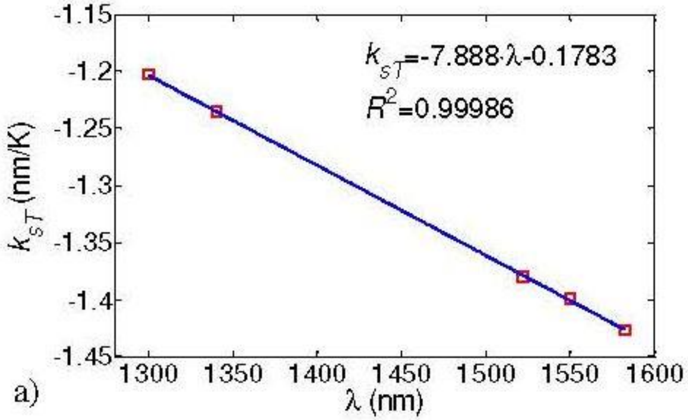

a)

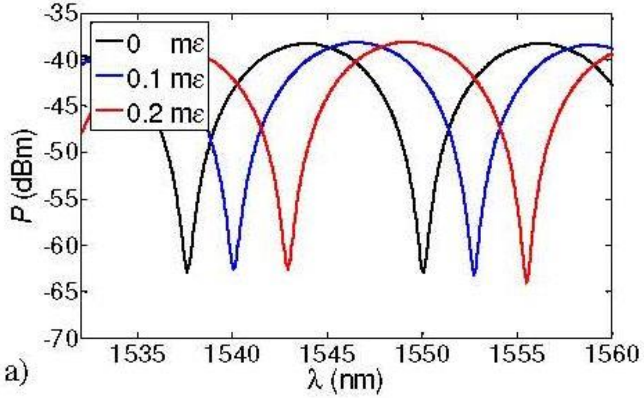

a)

$$\frac{d\Delta n}{dX} = \frac{d\lambda}{dX}\frac{\Delta n_G}{\lambda} - \frac{1}{L}\frac{dL}{dX}\Delta n$$

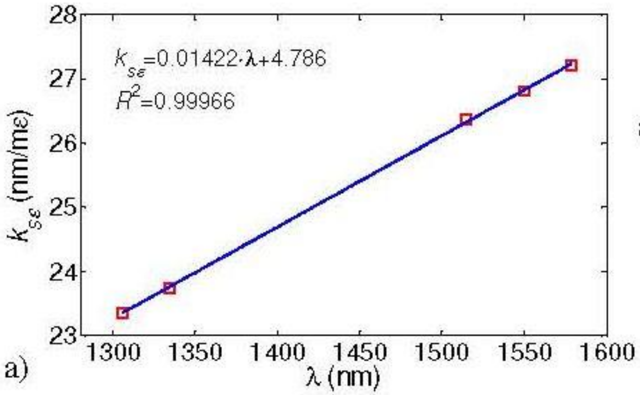

a)

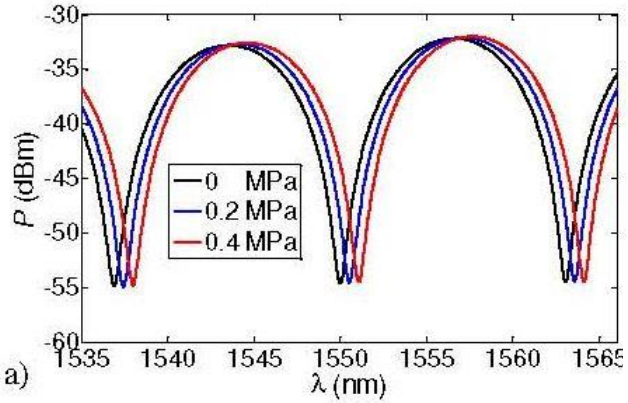

a)

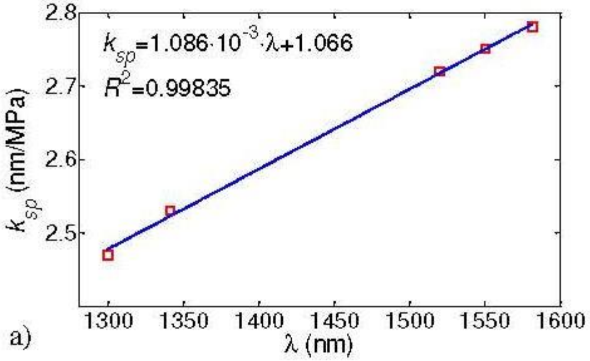

a)

Refractive index measurement

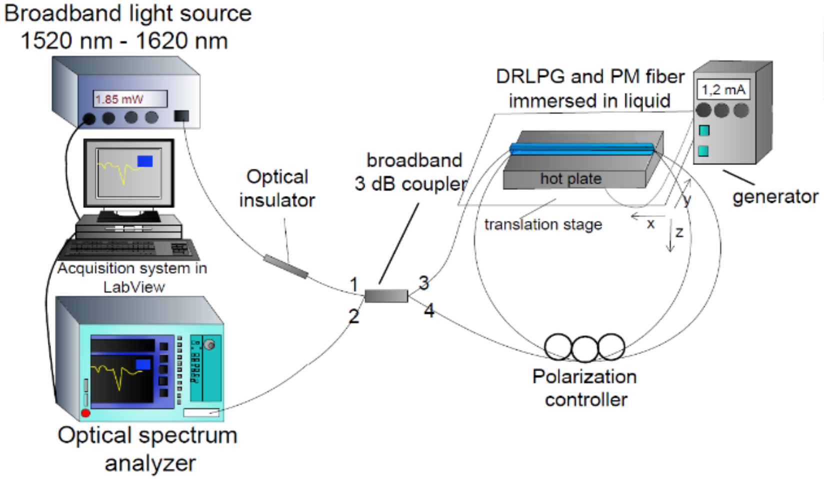

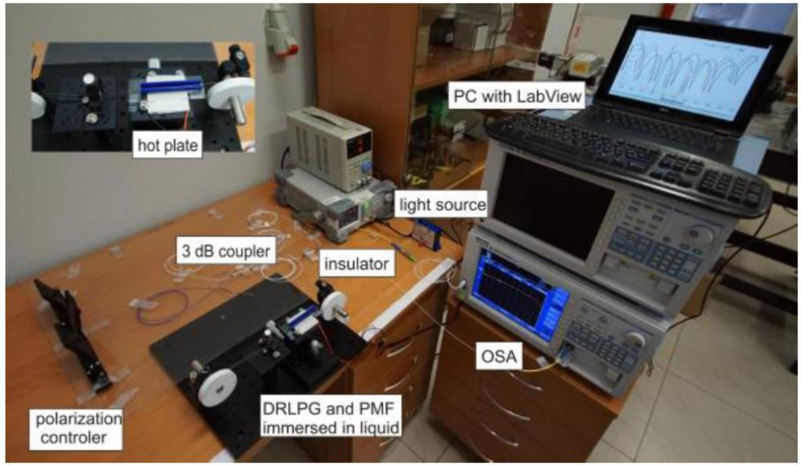

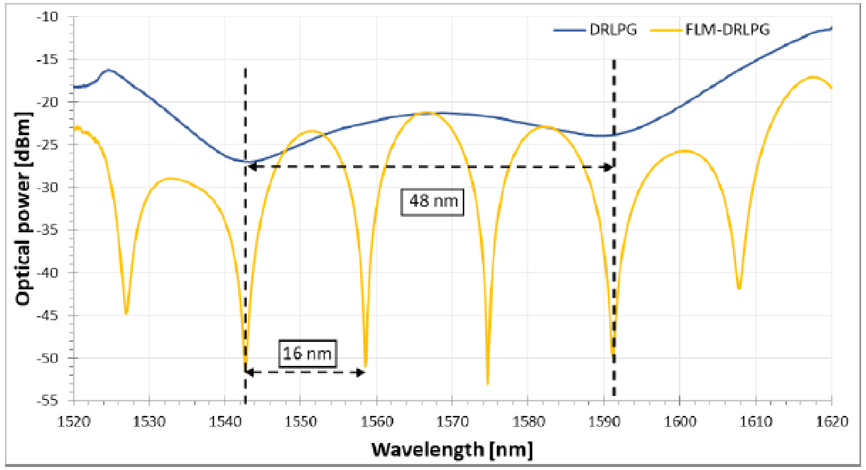

$$\begin{bmatrix}\Delta n\\ \Delta T\end{bmatrix} = \begin{bmatrix}1841.5\ (\mathrm{dB/RIU}) & 0.7304\ (\mathrm{dB/^\circ C})\\ 0 & 0.8562\ (\mathrm{dBm/^\circ C})\end{bmatrix}^{-1} \times \begin{bmatrix}\Delta P_{DRLPG}\\ \Delta P_{FLM}\end{bmatrix}$$

S=2375.8 dB/RIU for RI 1.333 – 1.341 and 1.1 dBm/^{o}C in range 23 – 41 ^{o}C

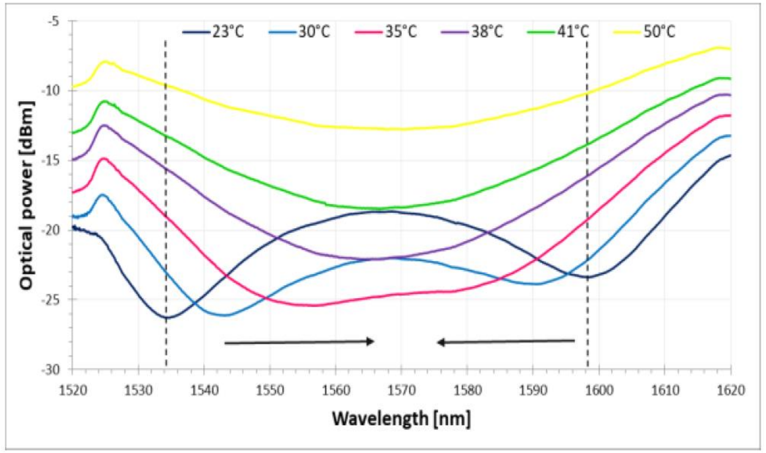

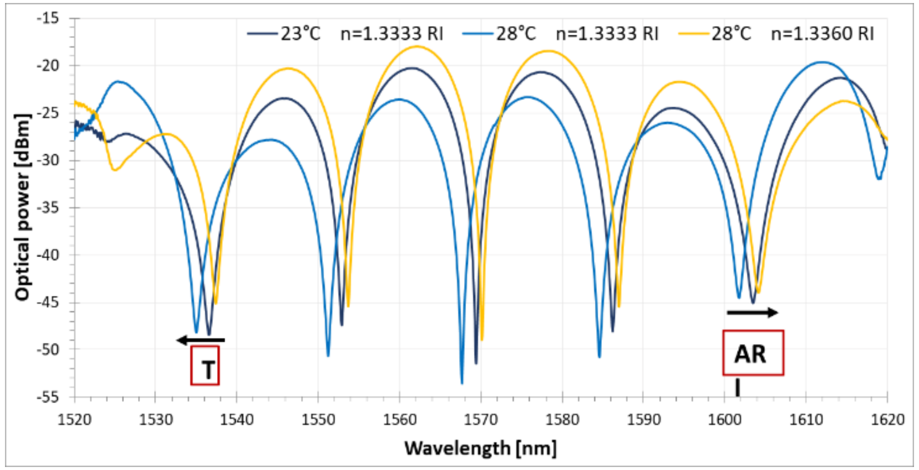

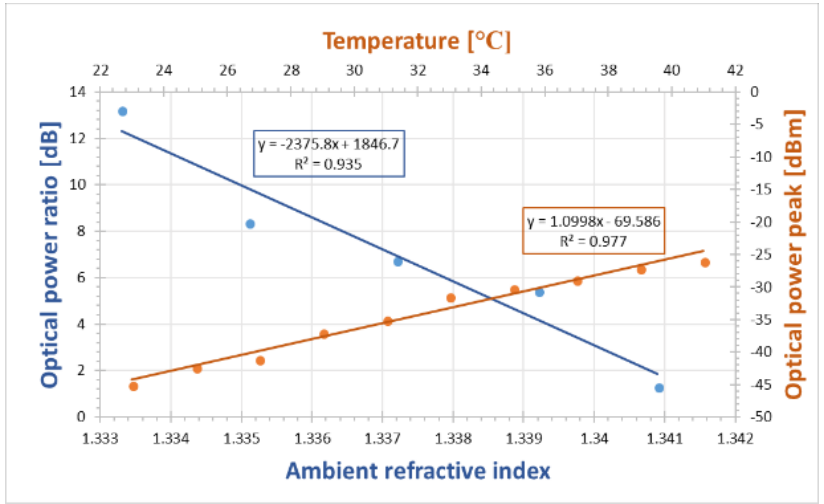

[Zawisza et al., *Sensors*, **18**, 2018, 2370]

Entanglement- enhanced optical gyro

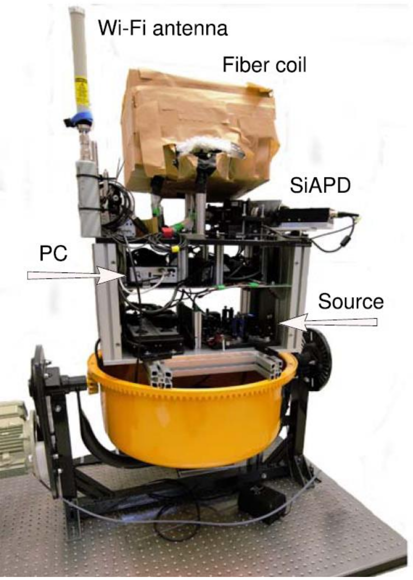

[Fink et al., *New J. Phys.*, **21**, 2019, 053010]

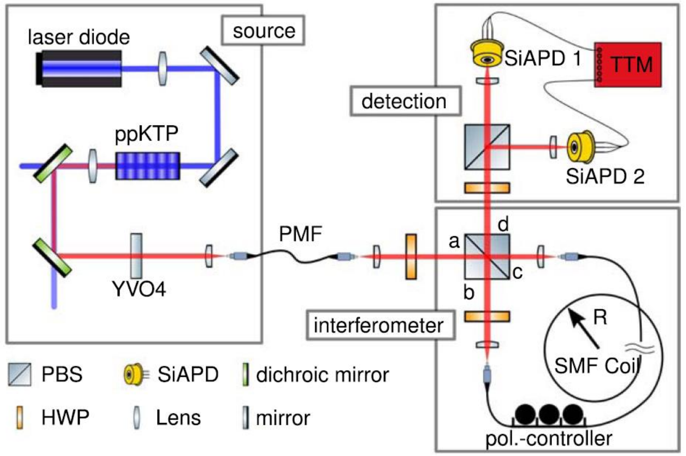

two-photon state $|\Psi^{\mathrm{PMF}}\rangle = |1_{\mathrm{H}}, 1_{\mathrm{V}}\rangle$

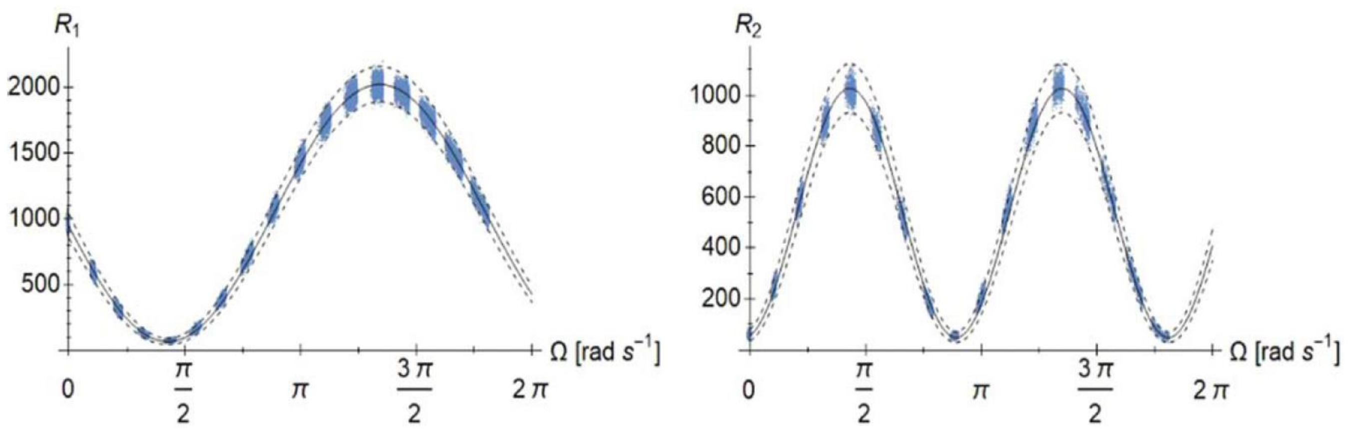

(a) $N = 1$ (b) $N = 2$

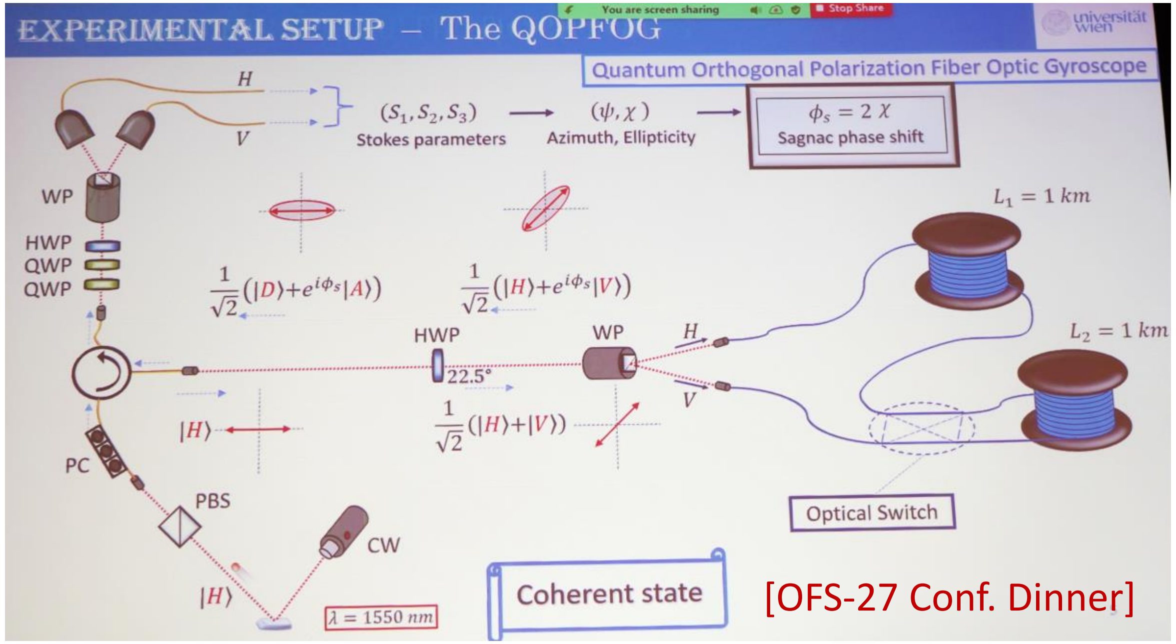

[OFS-27 Conf. Dinner]

Table 2. Comparison of the measurement precision with $M = 1955$ photons detected on average. Standard quantum limit $\Delta\Omega^{\mathrm{SNL}} = 1/(S\sqrt{M})$ and Heisenberg limit $\Delta\Omega^{\mathrm{HL}} = 1/(SM)$ of the measurement system, with the scale factor $S = 1.09$. Best precision of the respective measurement run $\Delta\Omega_{\min}$ (blue colored data in figure 4). Precision at the bias point $\Delta\Omega^{\mathrm{E}}_{\mathrm{Bias}}$, estimated via fit function. All values are given in rad s^{-1}.

N	$\Delta\Omega^{\mathrm{SNL}}$		$\Delta\Omega_{\min}$	$\Delta\Omega^{\mathrm{E}}_{\mathrm{Bias}}$		$\Delta\Omega^{\mathrm{HL}}$
1	0.0207	$\not>$	0.025(0)	0.024 8	>	469×10^{-6}
2		>	0.018(9)	0.018 3	>	

Thank you for your attention

this work has been made under financial suport National Center for Research and Development, Poland project – POIR.01.01.01-00-1553/20-00